Constrained Robust Model Reference Adaptive Control of a Tilt-Rotor Quadcopter Pulling an Unmodeled Cart

ROBERT B. ANDERSON
JULIUS A. MARSHALL
ANDREA L'AFFLITTO, Member, IEEE
Department of Industrial and Systems Engineering, Virginia Tech, Blacksburg, VA, USA

This article presents an innovative control architecture for tilt-rotor quadcopters with H-configuration transporting unknown, sling payloads. This control architecture leverages on a thorough analysis of the aircraft's equation of motion, which reveals gyroscopic effects that were not fully characterized and were disregarded while synthesizing control algorithms in prior publications. Furthermore, the proposed control architecture employs barrier Lyapunov functions and a novel robust model reference adaptive control law to guarantee *a priori* user-defined constraints on both the trajectory tracking error and the control input, despite poor information on the aircraft's inertial properties and the presence of unknown, unsteady payloads. Flight tests involving a quadcopter pulling an unmodeled cart by means of a thin rope of unknown length, which is slack at the beginning of the mission, verify the effectiveness of the theoretical results.

Manuscript received January 15, 2020; revised May 3, 2020; released for publication June 21, 2020. Date of publication July 10, 2020; date of current version February 9, 2021.

DOI. No. 10.1109/TAES.2020.3008575

Refereeing of this contribution was handled by G. Inalhan.

This work was supported by the US Army Research Lab, DARPA, and ONR under Grant 40304747, Grant D18AP00069, and Grant N000141912422.

Authors' addresses: Robert B. Anderson, Julius A. Marshall, and Andrea L'Afflitto are with the Department of Industrial and Systems Engineering, Virginia Tech, Blacksburg, VA 24061-1019 USA E-mail: (andersonb@vt.edu; mjulius@vt.edu; a.lafflitto@vt.edu). *(Corresponding author: Andrea L'Afflitto.)*

I. INTRODUCTION

Recently, a considerable growth of interest has arisen in the use of unmanned aerial vehicles (UAVs) employed in tasks different than remote sensing. These tasks, which are still considered as unconventional, range from payload delivery [1] to sensor placement [2], wall-climbing [3], shipboard landing [4], suspension bridge installation [5], window cleaning [6], and pushing payloads [7], [8]. In the future, UAVs will be also employed to transport unknown, sling payloads, and pull unmotorized carts. To enable these applications, the UAV's autopilots must guarantee satisfactory trajectory tracking performance also in the case the user does not have sufficient time or means to carefully measure the UAV's and payload's inertial properties or carefully tune the control laws. Motivated by this challenging task, this article presents a nonlinear robust control algorithm for tilt-rotor quadcopters with H-configuration, whose mission is to pull a cart along some arbitrary trajectory, while satisfying constraints on both the trajectory tracking error and the control input defined *a priori* by the user. The results presented in this article apply identically also to tilt-rotor UAVs lifting some sling payload.

In this article, we assume that the cart is connected to the aft of the UAV by means of a rope; (see Fig. 1). It is common practice to connect payloads to some location close to the UAV's center of mass. However, batteries and some sensors needed to accomplish the mission, such as altimeters and downward-facing cameras, may be located near the UAV's estimated center of mass. The results presented in this article can be seamlessly specialized to the case wherein the rope is connected at the UAV's estimated center of mass.

A tilt-rotor quadcopter with H-configuration has been chosen for its ability to exert horizontal forces without pitching and track arbitrary reference pitch and yaw angles at all time [9], [10]. Due to the underactuation of classical multirotor UAVs, the pitching moment needed to pull payloads connected to their aft could be particularly large, and thrust vectoring provides a technological solution to mitigate this effect. Indeed, as shown in [11], a conventional quadcopter may not be able to complete these kinds of missions.

The main challenges for the proposed control algorithm are three. First, it is assumed that both the UAV's and the cart's masses are known, but their inertia matrices and both the mass and the length of the rope connecting the aircraft to the cart are unknown. Therefore, both the inertia properties and the location of the center of mass of the overall mechanical system are unknown. The rationale for this modeling assumption is that the UAV's and payload's masses can be readily measured by means of weight scales. Both the position of the center of mass and the inertia matrix of rigid bodies can be estimated by some analytical or CAD (computer aided design) model, or can be measured experimentally. However, the implementation of analytical and CAD models may be time-consuming, and experimental rigs to measure inertia matrices are costly and need careful calibration [12]. The mass of the rope has been ignored,

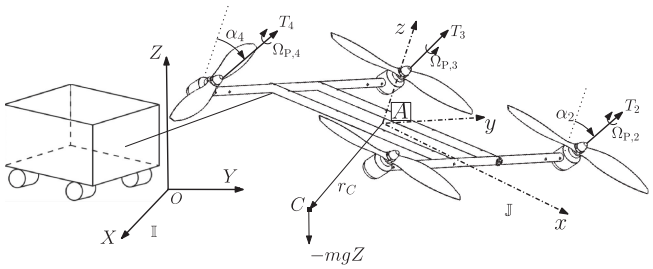

Fig. 1. Schematic representation of a tilt-rotor quadcopter pulling a cart by means of a thin rope connected to the edge of the aircraft.

since it is considered as a small fraction of the payload's mass, and its length has been ignored to relieve the user from the task of acquiring additional information. The second challenge for the proposed control algorithm is provided by the fact that the rope is slack at the beginning of the mission and is connected to the aft edge of the quadcopter. Therefore, as soon as the rope is taut, the aerial platform experiences both an impulsive force and an impulsive pitching moment, and the inertial properties of the overall mechanical system change instantaneously at a time instant that is unknown *a priori*. Finally, user-defined constraints on the control input challenge the ability of any control law to meet the constraints on the trajectory tracking error.

In the following, we outline the organization of this article. After having introduced the mathematical notation in Section II, Section III presents the equations of motion of a tilt-rotor quadcopter under the assumption that the vehicle's reference frame is centered at some user-defined point that does not coincide with the UAV's center of mass. This modeling choice couples the translational and rotational equations of motion and increases the computational cost of the corresponding control algorithm, but since the center of mass of the overall dynamical system is unknown and unsteady, this assumption is instrumental to increase the closed-loop system's robustness margins. Our analysis of the UAV's rotational dynamics reveals that the presence of tilting and spinning propellers, which are not aligned to one another, is captured by three terms, namely the inertial counter-torque, the gyroscopic effect, and an additional term that we named *tilt-rotor gyroscopic effect*. Both the inertial counter-torque and the gyroscopic effect characterize also the dynamics of conventional multirotor UAVs [13], whereas the tilt-rotor gyroscopic effect is identically equal to zero for classical multirotor UAVs because their propellers' spin axes are collinear to the UAV's vertical axis.

In Section IV, we exploit our analysis of the UAV's dynamic equations and design a control architecture for tilt-rotor quadcopters with H-configuration. According to this strategy, the reference trajectory, the reference pitch angle, and the reference yaw angle are user defined. The reference roll angle cannot be assigned by the user, but is deduced to satisfy the nonholonomic constraints given by the quadcopter's underactuation. Both the sum of propellers' thrust forces and the corresponding moments are considered as control inputs, and a feedback-linearizing control law introduces a proportional-derivative baseline controller in the closed-loop trajectory tracking error dynamics. Since the UAV's and the cart's inertial properties are unknown, the feedback-linearizing control law and the underlying proportional-derivative controller cannot guarantee satisfactory performance of the trajectory tracking error dynamics. To attain satisfactory performances, in this article, the baseline controller is augmented by some robust model reference adaptive control (MRAC) law. Since the proposed control architecture is modular, the proportional-derivative control law can be augmented by a control law designed according to any alternative control technique.

Existing results on the control of tilt-rotor aircraft rely on input–output linearization [14], robust output regularization [15], or state-feedback linearization together with proportional-derivative control [16], backstepping control [17], backstepping control with disturbance observers [18], sliding-mode control [19], hierarchical control [20], neural networks [21], geometric control [22], optimal control [23], or model predictive control [24]. Some authors exploit the differential flatness properties of tilt-rotor UAVs to design control laws [25]. However, the robustness margins provided by control laws based on proportional-derivative, backstepping, geometric, optimal, and feedback-linearizing frameworks are minimal. Control algorithms that implement hierarchical architectures are robust to matched and parametric uncertainties, but not unmatched uncertainties. Although neural networks provide a useful framework to design robust controls, larger unmatched uncertainties in the vehicle's dynamical model can be compensated by increasing the number of layers of the neural network. This approach, however, implies larger computational costs. Sliding mode control is a valuable nonlinear robust control technique. However, in our experience tuning these algorithms for quadcopter autopilot design is a more difficult task than tuning the adaptive rates for MRAC-based control algorithms for UAVs [13]. Robust MRAC laws, such as the one proposed in this article or the *e*-modification of MRAC [26], guarantee robustness not only to parametric and matched uncertainties, but also to unmatched uncertainties, and their computational complexity is irrespective of the unmatched uncertainties affecting the closed-loop system. In this article, no disturbance observer is employed to increase the closed-loop system's robustness margins; the only information on the effect of the cart on the vehicle's dynamics is provided by the measurements of its translational and rotational position and velocity. To the authors' best knowledge and according to a recent literature survey [27], a robust MRAC law has not been applied to design autopilots for tilt-rotor quadcopters.

MRAC laws guarantee asymptotic convergence of the trajectory tracking error in the presence of parametric and matched uncertainties, that is, uncertainties that can be parameterized by the regressor vector [28, Ch. 9, 11]. The feedback-linearizing control law presented in Section IV allows us to capture systematic errors in the estimation of the position of the quadcopter's center of mass and inertia

matrix as parametric uncertainties by means of a regressor vector and, hence, is particularly suitable to serve as a baseline controller for the MRAC laws; the analysis of the UAV's inertial counter-torque, gyroscopic effect, and tilt-rotor gyroscopic effect presented in Section III plays a pivotal role in the design of the regressor vector. Gyroscopic effects due to the tilting of the propellers' spin axes have been acknowledged by few other authors, but they have been neglected while designing control laws [29], [30]. Although this simplifying assumption is realistic for small UAVs, gyroscopic effects are more substantial for larger aircraft. To the authors' best knowledge, the proposed approach to design the regressor vector for a multirotor UAV's dynamic equations is unprecedented.

The last original contribution of Section IV consists of two alternative optimization-based strategies to compute each propeller's thrust force and spin axis' tilt angle so that the desired control input is realized. In particular, given the desired control input, that is, given the sum of the propellers' thrust forces and the corresponding moment, we compute each propeller's thrust force and spin axis' tilt angle both in the case all propellers are allowed to rotate independently and in the case all propellers' spin axes must be tilted by the same angle. Existing techniques to compute each propeller's thrust force and spin axis' tilt angle involve the control allocation technique [31] and the conditional distribution of the control parameters [32].

In Section V, we present a novel robust MRAC law to regulate the feedback-linearized equations of motion. This robust MRAC law exploits barrier Lyapunov functions to enforce user-defined constraints on both the trajectory tracking error and the adaptive gains at all time despite modeling errors, parameter estimation errors, and external disturbances. Remarkably, the proposed robust MRAC law enforces these constraints *a priori*, that is, no tuning is needed to meet user-defined specifications on the trajectory tracking error and the adaptive gains. If no user-defined constraints on the trajectory tracking error and the adaptive gains are imposed, then the MRAC law proposed in this article specializes to the *e*-modification of MRAC [26]. A classical approach to bound adaptive gains is to employ the projection operator [33], which constrains the adaptive gains within some user-defined convex set. However, using the projection operator one can only guarantee uniform ultimate boundedness of the trajectory tracking error, and the ultimate bounds can only be estimated in a conservative manner [34]. Only recently, barrier Lyapunov functions have been utilized to impose user-defined constraints on the closed-loop system's trajectory tracking error at all time [34]–[36], but in these cases, the adaptive gains are either unconstrained or constrained by employing the projection operator.

Finally, in Section VI, we present the results of flight tests achieved implementing the control architecture outlined in Section IV and the robust MRAC laws presented in Section V. In addition to the challenge of pulling an unknown cart, while satisfying user-defined constraints, the robustness of the proposed adaptive laws has been further strained by employing gain matrices in the feedback-linearized equations of motion, which have not been tuned in prior flight tests. Section VII synthesizes the main results of this article.

Preliminary results are presented in [37]. In this earlier work, only the results of numerical simulations are presented, the quadcopter is not challenged by any slung payload, the adaptive law involves 108 nonlinear coupled differential equations more than the adaptive law employed in this article, no comparison with other control techniques is presented, singularities in the reference roll angles are not considered, and the problem of realizing the desired forces and moments, while imposing that all propellers' tilt angles are equal to one another, is not addressed.

II. MATHEMATICAL NOTATION

In this section, we establish the notation used in this article. The set of *positive integers* is denoted by $\mathbb{N}$, the set of *real numbers* is denoted by $\mathbb{R}$, the set of $n \times 1$ *real column vectors* is denoted by $\mathbb{R}^n$, and the set of $n \times m$ *real matrices* is denoted by $\mathbb{R}^{n\times m}$. The *interior of the set* $\mathcal{S} \subseteq \mathbb{R}^{n\times m}$ is denoted by $\mathring{\mathcal{S}}$. The ith vector of the canonical basis in $\mathbb{R}^n$ is denoted by $\mathbf{e}_{i,n}$ or $\mathbf{e}_i$, the *identity matrix* in $\mathbb{R}^{n\times n}$ is denoted by $\mathbf{1}_n$, the *zero* $n \times m$ *matrix* in $\mathbb{R}^{n\times m}$ is denoted by $0_{n\times m}$ or 0.

We define $\mu_\kappa\colon \mathbb{R} \to \mathbb{R}$ so that $\mu_\kappa(\alpha) = \kappa \operatorname{sign}(\alpha)$ for $|\alpha| \leq \kappa$ and $\kappa > 0$, and $\mu_\kappa(\alpha) = \alpha$ for $|\alpha| > \kappa$, where $\operatorname{sign}(\cdot)$ denotes the signum function [38, p. 19]; it is worthwhile to note that the function $\mu_\kappa(\cdot)$ is piecewise continuously differentiable. Given $i \in \{1, \ldots, n\} \subset \mathbb{N}$, we define $\mathbf{I}_{i,n}\colon \mathbb{R}^n \to \mathbb{R}^n$ so that $\mathbf{e}_{j,n}^{\mathrm{T}}\mathbf{I}_{i,n}(x) = x_j$, $j \neq i$, and $\mathbf{e}_{i,n}^{\mathrm{T}}\mathbf{I}_{i,n}(x) = \mu_\kappa(x_i)$. Finally, we define $\widetilde{\mathbf{I}}_{i,n} : \mathbb{R}^n \to \mathbb{R}^n$ so that $\mathbf{e}_{j,n}^{\mathrm{T}}\widetilde{\mathbf{I}}_{i,n}(x) = x_j$, $j \neq i$, and $\mathbf{e}_{i,n}^{\mathrm{T}}\widetilde{\mathbf{I}}_{i,n}(x) = x_i - \mu_\kappa(x_i)$. Given $\alpha \in \mathbb{R}$, the trigonometric functions $\cos\alpha$, $\sin\alpha$, and $\tan\alpha$, are denoted by $\mathrm{c}\alpha$, $\mathrm{s}\alpha$, and $\mathrm{t}\alpha$, respectively.

The *transpose* of $B \in \mathbb{R}^{n\times m}$ is denoted by B^{T}, the *trace* of A is denoted by $\operatorname{tr}(A)$, and the smallest eigenvalue of the symmetric matrix $Q \in \mathbb{R}^{n\times n}$ is denoted by $\lambda_{\min}(Q)$. We write $\|\cdot\|$ both for the *Euclidean vector norm* and the corresponding *equi-induced matrix norm*, and we define $\|B\|_{\mathrm{F},L} \triangleq [\operatorname{tr}(BLB^{\mathrm{T}})]^{\frac{1}{2}}$ as the *weighted Frobenius norm* of $B \in \mathbb{R}^{n\times m}$, where $L \in \mathbb{R}^{m\times m}$ is symmetric and positive-definite; if $L = \mathbf{1}_m$, then we write $\|B\|_{\mathrm{F}}$. The *Kronecker product* of $A \in \mathbb{R}^{n\times m}$ and $B \in \mathbb{R}^{p\times q}$ is denoted by $A \otimes B$ [39, Def. 7.1.2]. Given $x \in \mathbb{R}^3$, we define the *cross-product operator* as $x^\times$.

III. KINODYNAMICS OF A TILT-ROTOR QUADCOPTER

In this section, we present the kinodynamic equations of a tilt-rotor quadcopter with H-configuration.

A. Modeling Assumptions and Dynamics' Notation

In order to deduce the quadcopter's kinodynamic equations, we consider both the aerial vehicle and its payload as a single mechanical system, which henceforth is referred to as the quadcopter. Furthermore, we assume that the UAV is

composed of a frame, which we model as a rigid body, and four propellers that can be independently tilted. Although the quadcopter's mass is assumed to be known, both the position of the quadcopter's center of mass and its inertia matrix are assumed to be unknown and unsteady.

Consider the orthonormal, inertial reference frame $\mathbb{I} \triangleq \{O; X, Y, Z\}$, centered in $O \in \mathbb{R}^3$, and with axes $X, Y, Z \in \mathbb{R}^3$. Consider also the orthonormal reference frame $\mathbb{J}(\cdot) \triangleq \{A(\cdot); x(\cdot), y(\cdot), z(\cdot)\}$ fixed with the vehicle's frame, centered at a point $A : [t_0, \infty) \to \mathbb{R}^3$ conveniently chosen, and with axes $x, y, z : [t_0, \infty) \to \mathbb{R}^3$; in this article, we refer to $\mathbb{J}(\cdot)$ as the *body reference frame*. If a vector $a \in \mathbb{R}^3$ is expressed in the reference frame $\mathbb{I}$, then it is denoted by $a^{\mathbb{I}}$; if a vector is expressed in $\mathbb{J}(\cdot)$, then no superscript is used. The *quadcopter's mass* is denoted by $m > 0$, and the gravitational acceleration is denoted by $g > 0$. The propellers' arms are aligned to the $y(\cdot)$ axis and $A(\cdot)$ does not coincide with the quadcopter's center of mass; for details, see Fig. 1.

The *position* of the reference point $A(\cdot)$ with respect to O is denoted by $r_A^{\mathbb{I}} : [t_0, \infty) \to \mathbb{R}^3$, and the *velocity* of $A(\cdot)$ with respect to the reference frame $\mathbb{I}$ is denoted by $v_A^{\mathbb{I}} : [t_0, \infty) \to \mathbb{R}^3$. Using a 3-2-1 rotation sequence, the orientation of $\mathbb{J}(\cdot)$ with respect to $\mathbb{I}$ is captured by the *roll angle* $\phi : [t_0, \infty) \to (-\frac{\pi}{2}, \frac{\pi}{2})$, the *pitch angle* $\theta : [t_0, \infty) \to (-\frac{\pi}{2}, \frac{\pi}{2})$, and the *yaw angle* $\psi : [t_0, \infty) \to [0, 2\pi)$ [40, pp. 11]. The *vector of independent generalized coordinates* is denoted by $q \triangleq [(r_A^{\mathbb{I}})^{\mathrm{T}}, \phi, \theta, \psi]^{\mathrm{T}} \in \mathcal{D}$, where $\mathcal{D} \triangleq \mathbb{R}^3 \times (-\frac{\pi}{2}, \frac{\pi}{2}) \times (-\frac{\pi}{2}, \frac{\pi}{2}) \times [0, 2\pi)$.

The propellers are centered at $r_{\mathrm{prop},1} = [L_x, -L_y, L_z]^{\mathrm{T}}$, $r_{\mathrm{prop},2} = [L_x, L_y, L_z]^{\mathrm{T}}$, $r_{\mathrm{prop},3} = [-L_x, -L_y, L_z]^{\mathrm{T}}$, and $r_{\mathrm{prop},4} = [-L_x, L_y, L_z]^{\mathrm{T}}$ with respect to the reference point $A(\cdot)$, where $L_x, L_y > 0$ and $L_z \geq 0$. The *angular position of the ith propeller about its spin axis* is denoted by $\Omega_i : [t_0, \infty) \to \mathbb{R}$, $i = 1, \ldots, 4$, and the *angular displacement of the ith propeller's spin axis about the* $y(\cdot)$ *axis*, measured from the $z(\cdot)$ axis, is denoted by $\alpha_i : [t_0, \infty) \to \mathbb{R}$. It is assumed that both $\alpha_i(\cdot)$, $i = 1, \ldots, 4$, and $\Omega_i(\cdot)$ can be estimated. The rotations about $x(\cdot)$, $y(\cdot)$, and $z(\cdot)$ axes of an angle $\alpha \in \mathbb{R}$ are captured by $R_x(\alpha), R_y(\alpha), R_z(\alpha) \in SO(3)$, respectively [40, p. 12], where $SO(n) \subset \mathbb{R}^{n \times n}$ denotes the *special orthogonal group in dimension n*.

B. Equations of Motion of a Tilt-Rotor Quadcopter

The *kinematic equations* of a tilt-rotor quadcopter are given by

$$\dot{q}(t) = \begin{bmatrix} v_A^{\mathbb{I}}(t) \\ \Gamma(q(t))\omega(q(t), \dot{q}(t)) \end{bmatrix}, \qquad q(t_0) = q_0, \qquad t \geq t_0 \tag{1}$$

where $\omega : \mathcal{D} \times \mathbb{R}^6 \to \mathbb{R}^3$ denotes the *angular velocity* of the reference frame $\mathbb{J}(\cdot)$ with respect to $\mathbb{I}$, and [40, Th. 1.7]

$$\Gamma(q) \triangleq \begin{bmatrix} 1 & \mathrm{s}\phi\,\mathrm{t}\theta & \mathrm{c}\phi\,\mathrm{t}\theta \\ 0 & \mathrm{c}\phi & -\mathrm{s}\phi \\ 0 & \mathrm{s}\phi\,\mathrm{c}^{-1}\theta & \mathrm{c}\phi\,\mathrm{c}^{-1}\theta \end{bmatrix}, \qquad q \in \mathcal{D}.$$

Furthermore, proceeding as in [41], one can prove that the *dynamic equations* of a tilt-rotor quadcopter are given by

$$\begin{aligned} &\mathcal{M}(t, q(t)) \begin{bmatrix} \dot{v}_A^{\mathbb{I}}(t) \\ \dot{\omega}(q(t), \dot{q}(t)) \end{bmatrix} \\ &\quad = \begin{bmatrix} f_{\mathrm{dyn,tran}}(t, q(t), \dot{q}(t)) \\ f_{\mathrm{dyn,rot}}(t, q(t), \dot{q}(t)) \end{bmatrix} + G(q(t))u(t) \\ &\quad \left[v_A^{\mathbb{I},\mathrm{T}}(t_0), \omega^{\mathrm{T}}(t_0)\right]^{\mathrm{T}} = \left[v_{A,0}^{\mathbb{I},\mathrm{T}}, \omega_0^{\mathrm{T}}\right]^{\mathrm{T}}, \qquad t \geq t_0 \end{aligned} \tag{2}$$

where

$$\begin{aligned} \mathcal{M}(t, q) &\triangleq \begin{bmatrix} m\mathbf{1}_3 & -mR(q)r_C^{\times}(t) \\ mr_C^{\times}(t)R^{\mathrm{T}}(q) & I(t) \end{bmatrix} \\ &\quad (t, q) \in [t_0, \infty) \times \mathcal{D} \end{aligned} \tag{3}$$

denotes the *generalized mass matrix*

$$\begin{aligned} f_{\mathrm{dyn,tran}}(t, q, \dot{q}) \triangleq\ & -mR(q)\left[\ddot{r}_C(t) + 2\omega^{\times}(q, \dot{q})\dot{r}_C(t)\right. \\ & \left. + \omega^{\times}(q, \dot{q})\omega^{\times}(q, \dot{q})r_C(t)\right] - mg\mathbf{e}_{3,3} \end{aligned} \tag{4}$$

$$\begin{aligned} f_{\mathrm{dyn,rot}}(t, q, \dot{q}) \triangleq\ & -\omega^{\times}(q, \dot{q})I(t)\omega(q, \dot{q}) - \dot{I}(t)\omega(q, \dot{q}) \\ & - \sum_{i=1}^{4}\left[I_{P_i}(t)\dot{\omega}_{P_i}(t)\right. \\ & \left. + \omega_{P_i}^{\times}(t)I_{P_i}(t)\omega_{P_i}(t)\right] \\ & - \omega^{\times}(q, \dot{q})\sum_{i=1}^{4} I_{P_i}(t)\omega_{P_i}(t) \\ & - mgr_C^{\times}(t)R^{\mathrm{T}}(q)\mathbf{e}_{3,3} \end{aligned} \tag{5}$$

$$G(q) \triangleq \begin{bmatrix} R(q)\begin{bmatrix}\mathbf{e}_{1,3} & \mathbf{e}_{3,3}\end{bmatrix} & 0_{3\times 3} \\ 0_{3\times 2} & \mathbf{1}_3 \end{bmatrix} \tag{6}$$

$R(q) \triangleq R_z(\psi)R_y(\theta)R_x(\phi)$, the unknown vector function $r_C : [t_0, \infty) \to \mathbb{R}^3$ denotes the position of the vehicle's center of mass with respect to the reference point $A(\cdot)$, the symmetric, positive-definite matrix function $I : [t_0, \infty) \to \mathbb{R}^{3\times 3}$ denotes the *inertia matrix* of the vehicle with respect to the reference point $A(\cdot)$, the symmetric, positive-definite matrix function $I_{P_i} : [t_0, \infty) \to \mathbb{R}^{3\times 3}$ denotes the *inertia matrix of the* ith *propeller*, $i = 1, \ldots, 4$, with respect to the reference point $A(\cdot)$, $\omega_{P_i} : [t_0, \infty) \to \mathbb{R}^3$ denotes the *angular velocity of the ith propeller with respect to the reference frame* $\mathbb{J}(\cdot)$, $u \triangleq [u_5, u_1, \ldots, u_4]^{\mathrm{T}} \in \mathbb{R}^5$ denotes the *control input*, $u_5, u_1 : [t_0, \infty) \to \mathbb{R}$ denote the components of the forces produced by the propellers along the $x(\cdot)$ and $z(\cdot)$ axes, respectively, and $[u_2, u_3, u_4]^{\mathrm{T}} : [t_0, \infty) \to \mathbb{R}^3$ denotes the moment of the force produced by the propellers; the first component of the control input $u(\cdot)$ is denoted by $u_5(\cdot)$ consistently with the literature on conventional multirotor UAVs, for which $u_5(t) \equiv 0, t \geq t_0$. We refer to (1) and (2) as the *quadcopter's equations of motion* or the *quadcopter's kinodynamic equations*.

REMARK 3.1 It follows from [40, Th. 1.3] that

$$\omega_{P_i}(t) = R_y(\alpha_i(t))\left[\dot{\Omega}_i(t)\mathbf{e}_{3,3} + \dot{\alpha}_i(t)\Omega_i(t)\mathbf{e}_{1,3}\right] \quad i = 1, \ldots, 4, \qquad t \geq t_0 \tag{7}$$

$$\dot{\omega}_{P_i}(t) = R_y(\alpha_i(t))\left[\ddot{\Omega}_i(t)\mathbf{e}_{3,3} + 2\dot{\alpha}_i(t)\dot{\Omega}_i(t)\mathbf{e}_{1,3} - \dot{\alpha}_i^2(t)\Omega_i(t)\mathbf{e}_{3,3} + \ddot{\alpha}_i(t)\Omega_i(t)\mathbf{e}_{1,3}\right] \tag{8}$$

and, applying the parallel axis theorem, the inertia matrix of the ith propeller, $i = 1, \ldots, 4$, is computed as

$$I_{P_i}(t) = R_y(\alpha_i(t))I_{\text{disk}}R_y^{\text{T}}(\alpha_i(t)) + m_{\text{prop}}r_{\text{prop},i}^{\text{T}}r_{\text{prop},i}\mathbf{1}_3 - m_{\text{prop}}r_{\text{prop},i}r_{\text{prop},i}^{\text{T}}, \qquad t \geq t_0 \tag{9}$$

where $I_{\text{disk}} \triangleq m_{\text{prop}}\rho_{\text{prop}}^2\text{diag}([0.25, 0.25, 0.50]^{\text{T}})$ denotes the inertia matrix of a thin disk of mass $m_{\text{prop}} > 0$ and radius $\rho_{\text{prop}} > 0$. The effect of the propellers' motion on a tilt-rotor quadcopter's dynamics is captured by $\sum_{i=1}^{4} I_{P_i}(\cdot)\dot{\omega}_{P_i}(\cdot)$, which is known as *inertial counter-torque*, $\omega^{\times}(\cdot)\sum_{i=1}^{4} I_{P_i}(\cdot)\omega_{P_i}(\cdot)$, which is known as *gyroscopic effect*, and $\sum_{i=1}^{4} \omega_{P_i}^{\times}(\cdot)I_{P_i}(\cdot)\omega_{P_i}(\cdot)$. Both the inertial counter-torque and the gyroscopic effect appear in the equations of motion of conventional quadcopters [41]. However, $\sum_{i=1}^{4} \omega_{P_i}^{\times}(t)I_{P_i}(t)\omega_{P_i}(t) \equiv 0$, $t \geq t_0$, for conventional quadcopters, since $\alpha_i(t) \equiv 0$, $i = 1, \ldots, 4$, $I_{P_i}(\cdot)$ is a diagonal matrix, and the propellers' thrust force is exerted along the $z(\cdot)$ axis of the reference frame $\mathbb{J}(\cdot)$. For the tilt-rotor quadcopter considered in this article, it holds that $\omega_{P_i}^{\times}(t)I_{P_i}(t)\omega_{P_i}(t) \not\equiv 0$, $t \geq t_0$, $i = 1, \ldots, 4$, since $\alpha_i(t) \not\equiv 0$. To the authors' best knowledge, existing results on tilt-rotor quadcopters do not account for the inertial counter-torque, the gyroscopic effect, or $\sum_{i=1}^{4} \omega_{P_i}^{\times}(\cdot)I_{P_i}(\cdot)\omega_{P_i}(\cdot)$, which will be henceforth referred to as the *tilt-rotor gyroscopic effect*.

Since the quadcopter's payload is considered as unsteady and the propellers' spin axes vary in time, the inertia matrix is a function of time that we model as

$$I(t) = I_{\text{quad}}(t) + \sum_{i=1}^{4} I_{P_i}(t), \qquad t \geq t_0 \tag{10}$$

where $I_{\text{quad}} : [t_0, \infty) \to \mathbb{R}^{3\times 3}$ is continuously differentiable and denotes the inertia matrix of the quadcopter, excluding its propellers, with respect to $A(\cdot)$. The quadcopter's dynamic equations involve the time derivative of the inertia matrix, and differentiating (9) and (10), we deduce that

$$\dot{I}(t) = \dot{I}_{\text{quad}}(t) + \sum_{i=1}^{4} \dot{\alpha}_i(t)R_y(\alpha_i(t))\left[\mathbf{e}_{2,3}^{\times}I_{\text{disk}} - I_{\text{disk}}\mathbf{e}_{2,3}^{\times}\right]R_y^{\text{T}}(\alpha_i(t)), \qquad t \geq t_0. \tag{11}$$

In the following section, we outline a control architecture for tilt-rotor quadcopters with H-configuration. This control architecture exploits our analysis of the aircraft dynamics to resolve the vehicle's underactuation and compute both the thrust force each propeller and the spin axis' tilt angle for each propeller so that the desired control input is realized.

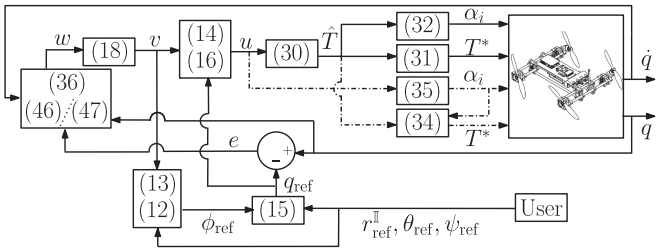

Fig. 2. Representation of the proposed control architecture for tilt-rotor quadcopters with H-configuration. The reference position $r_{\text{ref}}^{\mathbb{I}}(\cdot)$, the reference pitch angle $\theta_{\text{ref}}(\cdot)$, and the reference yaw angle $\psi_{\text{ref}}(\cdot)$ are user-defined. Since the vehicle is underactuated, the reference roll angle $\phi_{\text{ref}}(\cdot)$ is computed to realize the desired lateral force. The virtual control input $w(\cdot)$ regulates the closed-loop system's trajectory tracking error dynamics. Any control law can be used to compute $w(\cdot)$. In this article, $w(\cdot)$ is computed by applying the feedback control law (36) and either the original adaptive law (46) to enforce user-defined constraints or the classical adaptive law (47). The feedback control law (18) feedback-linearizes the UAV's equations of motion. The control input $u(\cdot)$ captures both the thrust force and the corresponding moment needed to follow the reference trajectory $q_{\text{ref}}(\cdot)$. If the propellers' tilt angles are chosen independently, then $\alpha_i(\cdot)$, $i = 1, \ldots 4$, is given by (32) and $T_i^*(\cdot)$ is given by (31). Alternatively, if the tilt angles must be equal to one another, then $\alpha_i(\cdot)$ is given by (35) and $T_i^*(\cdot)$ by (34).

IV. CONTROL ARCHITECTURE FOR TILT-ROTOR QUADCOPTERS

In this section, we present a control architecture that allows tilt-rotor quadcopters with H-configuration to follow some user-defined reference trajectory and attain some user-defined orientation. This architecture, which is captured by Fig. 2, comprises three major components. The first of these components provides a strategy to overcome the aircraft's underactuation and allows users to specify the UAV's reference trajectory, reference pitch angle, and reference yaw angle. The second component provides a strategy to feedback-linearize the UAV's equation of motion and reduce the trajectory tracking error dynamics to a form suitable for the implementation of MRAC laws. Finally, the third component provides two alternative strategies to determine the thrust force and the tilt angle for each propeller so that the desired forces and moments are produced. These three components of the proposed control architecture are discussed in Sections IV-A–IV-C below.

A. Solution of the Underactuation of Tilt-Rotors

By proceeding as in [13], we verify that quadcopters with H-configuration are underactuated, that is, are characterized by six degrees of freedom, namely the components of the vector of independent generalized coordinates $q(\cdot)$, and five control inputs, namely the components of control input $u(\cdot)$. To account for this limitation, the *reference trajectory* $r_{\text{ref}}^{\mathbb{I}} : [t_0, \infty) \to \mathbb{R}^3$, the *reference pitch angle* $\theta_{\text{ref}} : [t_0, \infty) \to (-\frac{\pi}{2}, \frac{\pi}{2})$, and the *reference yaw angle* $\psi_{\text{ref}} : [t_0, \infty) \to [0, 2\pi)$ are considered as user-defined, piecewise twice continuously differentiable, and bounded with their derivatives. The *reference roll angle* $\phi_{\text{ref}}(\cdot)$ is not

specified by the user, but is defined as

$$\phi_{\text{ref}}(t) \triangleq -\tan^{-1}\frac{\tilde{v}_{\text{tran},2}(t)}{\tilde{v}_{\text{tran},3}(t)}, \qquad t \geq t_0 \tag{12}$$

where $\tilde{v}_{\text{tran},2}(\cdot)$ and $\tilde{v}_{\text{tran},3}(\cdot)$ denote the second and the third components of

$$\tilde{v}_{\text{tran}}(t) \triangleq \mathbf{I}_{3,3}\left(R_y^{\text{T}}(\theta_{\text{ref}}(t))R_z^{\text{T}}(\psi_{\text{ref}}(t))v_{\text{tran}}(t)\right) \tag{13}$$

respectively, $\tan^{-1}(\cdot)$ denotes the *signed inverse tangent function*,

$$v_{\text{tran}}^{\mathbb{I}}(t) \triangleq R(q_{\text{ref}}(t))\left[u_5(t)\mathbf{e}_{1,3} + u_1(t)\mathbf{e}_{3,3}\right] \tag{14}$$

denotes the *translational equivalent control input*, and

$$q_{\text{ref}} \triangleq \left[\left(r_{\text{ref}}^{\mathbb{I}}\right)^{\text{T}}, \phi_{\text{ref}}, \theta_{\text{ref}}, \psi_{\text{ref}}\right]^{\text{T}} \in \mathbb{R}^6. \tag{15}$$

The *vector of reference generalized coordinates* $q_{\text{ref}}(\cdot)$ captures the state of an ideal quadcopter, whose underactuation is enforced by the nonholonomic constraint (12). The translational equivalent control input $v_{\text{tran}}^{\mathbb{I}}(\cdot)$ captures the thrust force that must be produced by the UAV propellers to follow the user-defined trajectory $q_{\text{ref}}(\cdot)$. The vector $\tilde{v}_{\text{tran}}(\cdot)$ captures the propellers' thrust force in a reference frame obtained by rotating the body reference frame $\mathbb{J}(\cdot)$ of an angle $\phi_{\text{ref}}(\cdot)$ about $x(\cdot)$ axis. Indeed, since tilt-rotor quadcopters with H-configuration can only produce thrust forces in the plane containing $x(\cdot)$ and $z(\cdot)$ axes of the body reference frame $\mathbb{J}(\cdot)$, the UAV must roll by an angle $\phi_{\text{ref}}(\cdot)$ to produce the thrust force required to translate laterally.

The proposed control architecture requires first to compute a feedback control law for the *equivalent control input*

$$v(t) \triangleq [v_{\text{tran}}^{\mathbb{I},\text{T}}(t), u_2(t), u_3(t), u_4(t)]^{\text{T}}, \qquad t \geq t_0 \tag{16}$$

so that the *trajectory tracking error* $e(t) \triangleq [q^{\text{T}}(t) - q_{\text{ref}}^{\text{T}}(t), \dot{q}^{\text{T}}(t) - \dot{q}_{\text{ref}}^{\text{T}}(t)]^{\text{T}}, t \geq t_0$, meets user-defined requirements. Successively, $\tilde{v}_{\text{tran}}(t)$, $t \geq t_0$, is computed by applying (13), and $\phi_{\text{ref}}(t)$ is computed from (12). Finally, $u_5(t)$, $t \geq t_0$, and $u_1(t)$ are computed from (14), and the control input $u(t)$ is reconstructed from (16). For details, see Fig. 2.

According to the definition of signed inverse tangent function, the reference roll angle $\phi_{\text{ref}}(\cdot)$ given by (12) is undefined whenever $\tilde{v}_{\text{tran},2}(t) = \tilde{v}_{\text{tran},3}(t) = 0$, $t \geq t_0$. However, $\mathbf{I}_{3,3}(\cdot)$ is defined so that if the third component of $R_y^{\text{T}}(\theta_{\text{ref}}(t))R_z^{\text{T}}(\psi_{\text{ref}}(t))v_{\text{tran}}(t)$, $t \geq t_0$, is arbitrarily small, that is, if $|\mathbf{e}_{3,3}^{\text{T}}R_y^{\text{T}}(\theta_{\text{ref}}(t))R_z^{\text{T}}(\psi_{\text{ref}}(t))v_{\text{tran}}^{\mathbb{I}}(t)| < \kappa$, where $\kappa > 0$ is user-defined, then $\tilde{v}_{\text{tran},3}(t) = \kappa\,\text{sign}(R_y^{\text{T}}(\theta_{\text{ref}}(t))R_z^{\text{T}}(\psi_{\text{ref}}(t))v_{\text{tran}}^{\mathbb{I}}(t))$. Therefore, $\phi_{\text{ref}}(\cdot)$ is always well defined. Furthermore, sensors used to measure the UAV's translational and rotational position and velocity are unavoidably affected by errors and hence, if the threshold parameter κ is smaller than the sensors' precision, then, in practice, $\mathbf{I}_{3,3}(R_y^{\text{T}}(\theta_{\text{ref}}(t))R_z^{\text{T}}(\psi_{\text{ref}}(t))v_{\text{tran}}^{\mathbb{I}}(t)) = R_y^{\text{T}}(\theta_{\text{ref}}(t))R_z^{\text{T}}(\psi_{\text{ref}}(t))v_{\text{tran}}^{\mathbb{I}}(t)$, $t \geq t_0$.

B. Feedback-Linearization of the Equations of Motion

In the following, we design a feedback control law for an equivalent control input $v(\cdot)$ given by (16) so that the equations of motion (1) and (2) are feedback-linearized, and the trajectory tracking error dynamics is reduced to a form that is suitable for MRAC laws. Specifically, we note that, by adding and subtracting $[v_{\text{tran}}^{\mathbb{I}}(t), 0_{1\times 3}]^{\text{T}}$, $t \geq t_0$, to the right-hand side of (2), where $v_{\text{tran}}^{\mathbb{I}}(\cdot)$ is given by (14), the tilt-rotor quadcopter's equations of motion (1) and (2) are equivalent to

$$\begin{aligned}
&\mathcal{M}(t, q(t))\begin{bmatrix}\mathbf{1}_3 & 0_{3\times 3}\\ 0_{3\times 3} & \Gamma^{-1}(q(t))\end{bmatrix}\ddot{q}(t)\\
&= \begin{bmatrix} f_{\text{dyn,tran}}(t, q(t), \dot{q}(t))\\ f_{\text{dyn,rot}}(t, q(t), \dot{q}(t))\end{bmatrix} + \left[G(q(t)) - G(q_{\text{ref}}(t))\right]u(t)\\
&\quad + \mathcal{M}(t, q(t))\begin{bmatrix} 0_{3\times 1}\\ \Gamma^{-1}(q(t))\dot{\Gamma}(q(t))\omega(q(t), \dot{q}(t))\end{bmatrix} + v(t)\\
&\left[q^{\text{T}}(t_0), \dot{q}^{\text{T}}(t_0)\right]^{\text{T}} = \left[q_0^{\text{T}}, q_{\text{d},0}^{\text{T}}\right]^{\text{T}}, \qquad t \geq t_0
\end{aligned} \tag{17}$$

and considering $v(\cdot)$ as the control input for (17), this dynamical system is fully actuated. Therefore, we design a feedback control law for $v(\cdot)$ so that (17) is feedback-linearized, and the trajectory tracking error $e(\cdot)$ meets user-defined requirements at all times.

The feedback-linearizing control law for $v(\cdot)$ is introduced by the next theorem. For the statement of this result, let $\overline{r}_C(\cdot)$ and $\overline{I}(\cdot)$ denote estimates of the unknown terms $r_C(\cdot)$ and $I(\cdot)$, respectively, and let $\overline{\mathcal{M}}(\cdot,\cdot)$, $\overline{f}_{\text{dyn,tran}}(\cdot,\cdot,\cdot)$, and $\overline{f}_{\text{dyn,rot}}(\cdot,\cdot,\cdot)$ denote estimates of $\mathcal{M}(\cdot,\cdot)$, $f_{\text{dyn,tran}}(\cdot,\cdot,\cdot)$, and $f_{\text{dyn,rot}}(\cdot,\cdot,\cdot)$, respectively, which are deduced from (3)–(5) by substituting $r_C(\cdot)$ and $I(\cdot)$ with $\overline{r}_C(\cdot)$ and $\overline{I}(\cdot)$, respectively. Both $\overline{r}_C(\cdot)$ and $\overline{I}(\cdot)$ are designed so that both $\overline{I}(\cdot)$ and $\overline{\mathcal{M}}(\cdot,\cdot)$ are positive-definite, and can be deduced, for example, using analytical models of the vehicle's configuration. Let $\Delta\mathcal{M}(\cdot,\cdot)$, $\Delta f_{\text{dyn,tran}}(\cdot,\cdot,\cdot)$, and $\Delta f_{\text{dyn,rot}}(\cdot,\cdot,\cdot)$ capture unmatched uncertainties on the generalized mass matrix and the UAV's inertial forces so that $\mathcal{M}(t,q) = \overline{\mathcal{M}}(t,q) + \Delta\mathcal{M}(t,q)$, $(t,q,\dot{q}) \in [t_0,\infty)\times\mathcal{D}\times\mathbb{R}^6$, $f_{\text{dyn,tran}}(t,q,\dot{q}) = \overline{f}_{\text{dyn,tran}}(t,q,\dot{q}) + \Delta f_{\text{dyn,tran}}(t,q,\dot{q})$, and $f_{\text{dyn,rot}}(t,q,\dot{q}) = \overline{f}_{\text{dyn,rot}}(t,q,\dot{q}) + \Delta f_{\text{dyn,rot}}(t,q,\dot{q})$. Finally, let $\overline{\overline{r}}_C \in \mathbb{R}^3$ be unknown and let $\overline{\overline{I}} \in \mathbb{R}^{3\times 3}$ be symmetric, positive-definite, and unknown so that $\overline{\overline{r}}_C$ and $\overline{\overline{I}}$ capture systematic errors in the estimation of the position of the quadcopter's center of mass and inertia matrix, respectively, and let $\overline{\overline{f}}_{\text{dyn,tran}}(q,\dot{q}) \triangleq -mR(q)\omega^{\times}(q,\dot{q})\omega^{\times}(q,\dot{q})\overline{\overline{r}}_C$, $(t,q,\dot{q}) \in [t_0,\infty)\times\mathcal{D}\times\mathbb{R}^6$, and $\overline{\overline{f}}_{\text{dyn,rot}}(q,\dot{q}) \triangleq -\omega^{\times}(q,\dot{q})\overline{\overline{I}}\omega(q,\dot{q}) - mg\overline{\overline{r}}_C^{\times}R^{\text{T}}(q)\mathbf{e}_{3,3}$. The unknown functions $\overline{\overline{f}}_{\text{dyn,tran}}(q,\dot{q})$, $(q,\dot{q}) \in \mathcal{D}\times\mathbb{R}^6$, and $\overline{\overline{f}}_{\text{dyn,rot}}(q,\dot{q})$ capture parametric uncertainties and approximate $\Delta f_{\text{dyn,tran}}(\cdot,\cdot,\cdot)$ and $\Delta f_{\text{dyn,rot}}(\cdot,\cdot,\cdot)$, respectively. Accounting for parametric uncertainties is advantageous since the robustness margins of MRAC laws, such as those employed in this article, are reduced by unmatched uncertainties, but not by parametric and matched uncertainties [28, Ch. 9, 11].

THEOREM 4.1 Consider the nonlinear dynamical system (17) and the feedback control law

$$\begin{aligned}
&\beta(t, q, q_{\mathrm{ref}}, w)\\
&\triangleq \mathbf{I}_{3,6}\Bigg(\overline{\mathcal{M}}(t, q)\begin{bmatrix}\mathbf{1}_3 & 0_{3\times 3}\\ 0_{3\times 3} & \Gamma^{-1}(q)\end{bmatrix}\Bigg[\ddot{q}_{\mathrm{ref}} - \begin{bmatrix}0_{3\times 1}\\ \dot{\Gamma}(q)\omega(q,\dot{q})\end{bmatrix}\\
&\quad - [K_{\mathrm{P}}, K_{\mathrm{D}}]\begin{bmatrix}q - q_{\mathrm{ref}}\\ \dot{q} - \dot{q}_{\mathrm{ref}}\end{bmatrix} - \Theta^{\mathrm{T}}\Phi(q,\dot{q}) + w\Bigg]\\
&\quad - \begin{bmatrix}\overline{f}_{\mathrm{dyn,tran}}(t, q, \dot{q})\\ \overline{f}_{\mathrm{dyn,rot}}(t, q, \dot{q})\end{bmatrix}\Bigg),\\
&\qquad (t, q, q_{\mathrm{ref}}, w) \in [t_0, \infty) \times \mathcal{D} \times \mathbb{R}^6 \times \mathbb{R}^6 \qquad (18)
\end{aligned}$$

where K_{P} and $K_{\mathrm{D}} \in \mathbb{R}^{6\times 6}$ are symmetric and positive-definite, $\Theta^{\mathrm{T}} = \begin{bmatrix}\Theta_{\mathrm{tran}} & 0_{3\times 30}\\ 0_{3\times 9} & \Theta_{\mathrm{rot}}\end{bmatrix}$, $\Phi(q,\dot{q}) = [\Phi_{\mathrm{tran}}^{\mathrm{T}}(q,\dot{q}), \Phi_{\mathrm{rot}}^{\mathrm{T}}(q,\dot{q})]^{\mathrm{T}}$,

$$\Theta_{\mathrm{tran}} = M_W(\overline{\overline{r}}_C, 3) \qquad (19)$$

$$\Theta_{\mathrm{rot}} = \left[M_W\left(W_M(\overline{\overline{I}}), 3\right), \overline{\overline{r}}_C^{\times}\right] \qquad (20)$$

$$\Phi_{\mathrm{tran}}(q,\dot{q}) = -mW_M(R(q)\omega^{\times}(q,\dot{q})\omega^{\times}(q,\dot{q})) \qquad (21)$$

$$\begin{aligned}
\Phi_{\mathrm{rot}}(q,\dot{q}) = \Big[&- W_M^{\mathrm{T}}\left(\omega^{\times}(q,\dot{q})M_W(\omega(q,\dot{q}))\right)\\
&- mg\mathbf{e}_{3,3}^{\mathrm{T}}R(q)\Big]^{\mathrm{T}} \qquad (22)
\end{aligned}$$

$$M_W(b, n) \triangleq b^{\mathrm{T}} \otimes \sum_{i=1}^{n} \mathbf{e}_{i,n}, \qquad (b, n) \in \mathbb{R}^m \times \mathbb{N} \qquad (23)$$

$$W_M(A) \triangleq \sum_{i=1}^{n}\left[\mathbf{e}_{i,m} \otimes \left(A\mathbf{e}_{i,m}\right)\right], \qquad A \in \mathbb{R}^{n\times m}. \qquad (24)$$

If $v(t) = \beta(t, q(t), q_{\mathrm{ref}}(t), w(t))$, then (17) is equivalent to

$$\begin{aligned}
&\dot{e}(t) = A_{\mathrm{ref}}e(t) + B\left[w(t) + \Theta^{\mathrm{T}}\Phi(q(t),\dot{q}(t))\right] + \xi(t)\\
&e(t_0) = \begin{bmatrix}q_0\\ q_{\mathrm{d},0}\end{bmatrix} - \begin{bmatrix}q_{\mathrm{ref}}(t_0)\\ \dot{q}_{\mathrm{ref}}(t_0)\end{bmatrix}, \qquad t \geq t_0 \qquad (25)
\end{aligned}$$

where $A_{\mathrm{ref}} \triangleq \begin{bmatrix}0_{6\times 6} & \mathbf{1}_6\\ -K_{\mathrm{P}} & -K_{\mathrm{D}}\end{bmatrix}$, $B \triangleq \begin{bmatrix}0_{6\times 6}\\ \mathbf{1}_6\end{bmatrix}$, $\xi(t) = [0_{1\times 6}, \xi_{\mathrm{dyn}}^{\mathrm{T}}(t)]^{\mathrm{T}} \in \mathbb{R}^{12}$, and

$$\begin{aligned}
\xi_{\mathrm{dyn}}(t) = \widetilde{\mathbf{I}}_{3,6}\Bigg(&\begin{bmatrix}\mathbf{1}_3 & 0_{3\times 3}\\ 0_{3\times 3} & \Gamma(q(t))\end{bmatrix}\overline{\mathcal{M}}^{-1}(t, q)\\
&\cdot\Bigg(\begin{bmatrix}\Delta f_{\mathrm{dyn,tran}}(t, q, \dot{q})\\ \Delta f_{\mathrm{dyn,rot}}(t, q, \dot{q})\end{bmatrix} + \left[G(q(t)) - G(q_{\mathrm{ref}}(t))\right]u(t)\\
&-\Delta\mathcal{M}(t, q)\begin{bmatrix}\mathbf{1}_3 & 0_{3\times 3}\\ 0_{3\times 3} & \Gamma^{-1}(q(t))\end{bmatrix}\ddot{q}(t)\Bigg)\Bigg) \qquad (26)
\end{aligned}$$

PROOF Since $Ab = M_W(b, n)W_M(A)$, $(n, A, b) \in \mathbb{N} \times \mathbb{R}^{n\times m} \times \mathbb{R}^m$, it holds that $\Theta^{\mathrm{T}}\Phi(q,\dot{q}) = \begin{bmatrix}\overline{\overline{f}}_{\mathrm{dyn,tran}}(q,\dot{q})\\ \overline{\overline{f}}_{\mathrm{dyn,rot}}(q,\dot{q})\end{bmatrix}$, $(q,\dot{q}) \in \mathcal{D} \times \mathbb{R}^6$. Thus, (25) and (26) directly follow from (17) with $v(t) = \beta(t, q(t), q_{\mathrm{ref}}(t), w(t)), t \geq t_0$. ■

The feedback-linearizing control law (18) reduces the trajectory tracking error dynamics to a linear, controllable dynamical system, which is captured by (25), is regulated by the *virtual control input* $w(\cdot)$, and is perturbed by $\xi(\cdot)$. In particular, (18) exploits the estimated quantities $\overline{\mathcal{M}}(\cdot,\cdot)$, $\overline{f}_{\mathrm{dyn,tran}}(\cdot,\cdot,\cdot)$, and $\overline{f}_{\mathrm{dyn,rot}}(\cdot,\cdot,\cdot)$ to attempt to cancel the coupling terms in (17) and introduces a proportional-derivative control law with gains K_{P} and K_{D}, which serves as a baseline controller for $w(\cdot)$. The term $\xi(\cdot)$ in (25) accounts for unmatched uncertainties, including the presence of an unsteady payload whose inertial properties are unknown. Any linear or nonlinear robust control law for $w(\cdot)$ can be designed so that the trajectory tracking error $e(\cdot)$ meets user-defined levels of performance, and as discussed in Section V below, in this article, we employ MRAC laws to design the virtual control input. Since the robustness of MRAC laws is unaffected by parametric uncertainties [28, Ch. 11], the feedback control law (18) introduces the term $\Theta^{\mathrm{T}}\Phi(q,\dot{q})$, $(q,\dot{q}) \in \mathcal{D} \times \mathbb{R}^6$, in (25) to explicitly account for parametric uncertainties and counteract the destabilizing effect of the unmatched uncertainties. MRAC laws usually produce strong control inputs in the presence of large trajectory tracking errors and induce large oscillations of the trajectory tracking error during the transient phase. The proportional-derivative baseline controller allows the MRAC law for $w(\cdot)$ to be less aggressive.

Vehicles that are controlled by a thrust force along a single direction and that have full torque actuation for attitude control, such as quadcopters, are limited by the fact that if $\ddot{r}_{\mathrm{ref}}^{\mathbb{I}}(t) = -g\mathbf{e}_{3,3} - \ddot{r}_C^{\mathbb{I}}(t)$, $t \geq t_0$, then a control law may not be defined [42], [43]. For the tilt-rotor quadcopter considered in this article, this condition is verified if and only if the UAV does not produce any thrust force along the Z axis of the inertial reference frame $\mathbb{I}$, and is in free fall. Now, (16) and (14) imply that the third component of $v(\cdot)$ captures the component of the propellers' thrust force along the Z axis of the inertial reference frame $\mathbb{I}$. Therefore, the feedback control law (18) embeds the function $\mathbf{I}_{3,6}(\cdot)$ so that if $v(t) = \beta(t, q(t), q_{\mathrm{ref}}(t), w(t))$, $t \geq t_0$, then $\mathbf{e}_{3,6}^{\mathrm{T}}v(t) \neq 0$ and the closed-loop system is controllable at all times. Motors for UAVs are unable to produce arbitrarily small thrust force and suffer from small, but not zero, error in tilting the propellers. Thus, if κ is sufficiently small, then in practice the discontinuity produced by $\mathbf{I}_{3,6}(\cdot)$ in the time derivative of the baseline control law $\beta(\cdot,\cdot,\cdot,\cdot)$ is negligible.

C. Realization of the Desired Control Inputs

Once the virtual control input $w(\cdot)$ has been computed, (17) is feedback-linearized by setting $v(t) = \beta(t, q(t), q_{\mathrm{ref}}(t), w(t))$, $t \geq t_0$, and the control input $u(\cdot)$ is computed from (14) and (16), the forces and moments needed for $q(\cdot)$ to track $q_{\mathrm{ref}}(\cdot)$ must be realized by generating the appropriate thrust forces $T_i(\cdot)$, $i = 1, \ldots, 4$, and tilting the propellers' axes by $\alpha_i(\cdot)$. In this section, we present two optimization-based approaches that provide $T_i(\cdot)$, $i = 1, \ldots, 4$, and $\alpha_i(\cdot)$ assuming that the propellers' axes tilt angles are either independent from one another or equal

to one another. To achieve these results, we model the ith propeller's thrust force as

$$T_i(t) = k\dot{\Omega}_i^2(t), \qquad i = 1, \ldots, 4, \qquad t \geq t_0 \tag{27}$$

where $k > 0$, and we model the moment of the aerodynamic drag induced by the ith propeller as

$$D_i(t) = k_{\mathrm{T}} T_i(t) \tag{28}$$

where $k_{\mathrm{T}} > 0$ [13]. Furthermore, we assume that adjacent propellers spin in opposite directions so that

$$u(t) = QA(\alpha(t))T(t), \qquad t \geq t_0 \tag{29}$$

where $T(t) \triangleq [T_1(t), T_2(t), T_3(t), T_4(t)]^{\mathrm{T}} \in \mathbb{R}^4$ denotes the *vector of thrust forces*, $\alpha \triangleq [\alpha_1(t), \alpha_2(t), \alpha_3(t), \alpha_4(t)]^{\mathrm{T}} \in \mathbb{R}^4$, $\alpha \triangleq [\alpha_1(t), \alpha_2(t), \alpha_3(t), \alpha_4(t)]^{\mathrm{T}} \in \mathbb{R}^4$

$$Q \triangleq \begin{bmatrix} 0 & 1 & 0 & 1 & 0 & 1 & 0 & 1 \\ 1 & 0 & 1 & 0 & 1 & 0 & 1 & 0 \\ L_y & k_{\mathrm{T}} & L_y & -k_{\mathrm{T}} & -L_y & k_{\mathrm{T}} & -L_y & -k_{\mathrm{T}} \\ -L_x & L_z & L_x & L_z & L_x & L_z & -L_x & L_z \\ k_{\mathrm{T}} & -L_y & -k_{\mathrm{T}} & -L_y & k_{\mathrm{T}} & L_y & -k_{\mathrm{T}} & L_y \end{bmatrix}$$

and $A(\alpha) \in \mathbb{R}^{8\times 4}$ is such that the element on its $(2i-1)$th row and ith column, $i = 1, \ldots, 4$, is given by $\mathrm{c}\alpha_i$, the element on its $2i$th row and ith column is given by $\mathrm{s}\alpha_i$, and every other element is equal to zero.

The next theorem presents the first of the two optimization-based approaches discussed in this section to compute each propeller's thrust force and spin axes' tilt angle. For the proof of this result, we note that Q is full-rank, since $L_x L_y > 0$ and $k_{\mathrm{T}} > 0$, and hence, its *Moore–Penrose inverse* is given by $Q^+ \triangleq Q^{\mathrm{T}}[QQ^{\mathrm{T}}]^{-1}$. Furthermore, we recall that there are infinitely many solutions to the problem of finding $\tilde{T} : [t_0, \infty) \to \mathbb{R}^8$ such that $\|Q\tilde{T}(t) - u(t)\|^2$, $t \geq t_0$, is minimized, and the solution with smallest Euclidean norm is given by [44, p. 649]

$$\hat{T}(t) \triangleq Q^+ u(t). \tag{30}$$

THEOREM 4.2 Consider the linear system (29) and assume that $u : [t_0, \infty) \to \mathbb{R}^5$ is given. If

$$T_i^*(t) = \sqrt{\hat{T}_{2i-1}^2(t) + \hat{T}_{2i}^2(t)}, \quad i = 1, \ldots, 4, \quad t \geq t_0 \tag{31}$$

$$\alpha_i(t) = \tan^{-1} \frac{\hat{T}_{2i}(t)}{\hat{T}_{2i-1}(t)} \tag{32}$$

where $\hat{T}(t)$ is given by (30), then

$$T^*(t) = \arg\min_{T\in\mathbb{R}^4} \|QA(\alpha(t))T - u(t)\| \tag{33}$$

where $T^*(t) = [T_1^*(t), T_2^*(t), T_3^*(t), T_4^*(t)]^{\mathrm{T}}$.

PROOF Let $T^* : [t_0, \infty) \to \mathbb{R}^4$ be such that $\hat{T}(t) = A(\alpha(t))T^*(t)$, $t \geq t_0$, where $\hat{T}(t)$ is given by (30). Equations (31) and (32) directly follow from the fact that the $(2i-1)$th, $i = 1, \ldots, 4$, and the $2i$th component of $\hat{T}(\cdot)$ capture the components of $T^*(\cdot)$ along $z(\cdot)$ and $x(\cdot)$ axes of the body reference frame $\mathbb{J}(\cdot)$, respectively. Finally, (33) follows from the fact that $\|QA(\alpha(t))T^*(t) - u(t)\|^2 = \|Q\hat{T}(t) - u(t)\|^2 \leq \|Q\tilde{T}(t) - u(t)\|^2$ for all $t \geq t_0$ and all $\tilde{T} : [t_0, \infty) \to \mathbb{R}^8$. ■

The next result provides a simpler alternative to Theorem 4.2. Specifically, in this theorem, we deduce the thrust force each propeller must produce to realize the desired control input $u(\cdot)$, assuming that all spin axes tilt by the same angle, that is, $\alpha_1(t) = \cdots = \alpha_4(t)$, $t \geq t_0$.

THEOREM 4.3 Consider the linear system (29) and assume that $u : [t_0, \infty) \to \mathbb{R}^5$ is given and $\alpha_1(t) = \cdots = \alpha_4(t)$, $t \geq t_0$. If

$$T_i^*(t) = \left[\hat{T}_{2i-1}(t), \hat{T}_{2i}(t)\right][\mathrm{c}\alpha_i(t), \mathrm{s}\alpha_i(t)]^{\mathrm{T}} \qquad i = 1, \ldots, 4, \qquad t \geq t_0 \tag{34}$$

$$\alpha_i(t) = \tan^{-1} \frac{u_5(t)}{u_1(t)} \tag{35}$$

where $\hat{T}(t) = Q^+ u(t)$, then (33) is verified.

PROOF Equation (35) follows from the facts that $\alpha_1(t) = \cdots = \alpha_4(t)$, $t \geq t_0$, and that $u_5(\cdot)$ and $u_1(\cdot)$ denote the components of the forces produced by the propellers along $x(\cdot)$ and $z(\cdot)$ axes, respectively. Now, as discussed in the proof of Theorem 4.2, $\hat{T}(t) = Q^+ u(t)$, $t \geq t_0$, minimizes $\|Q\tilde{T} - u(t)\|^2$ over all $\tilde{T} \in \mathbb{R}^8$. Furthermore, the objective function $\|QA(\alpha(t))T - u(t)\|^2$, $t \geq t_0$, is convex on $\mathbb{R}^4$, and hence, all its minimizers are global minimizers. Therefore, since $A(\alpha(t))T = T \otimes [\mathrm{c}\alpha_i(t), \mathrm{s}\alpha_i(t)]^{\mathrm{T}}$, $T \in \mathbb{R}^4$, $t \geq t_0$, finding $T^*(t)$, $t \geq t_0$, that verifies (33) is equivalent to finding a global minimizer of $\mathcal{L}(T(\cdot)) \triangleq \|T(t) \otimes [\mathrm{c}\alpha_i(t), \mathrm{s}\alpha_i(t)]^{\mathrm{T}} - \hat{T}(t)\|^2$. Necessary and sufficient condition to minimize $\mathcal{L}(T)$ over all $T \in \mathbb{R}^4$ is that $\frac{\partial \mathcal{L}(T)}{\partial T} = 0$. Since, $\frac{\partial \mathcal{L}(T)}{\partial T} = T - p(\hat{T})$, where $p(\hat{T}(t)) \triangleq \begin{bmatrix} \hat{T}_1(t) & \hat{T}_3(t) & \hat{T}_5(t) & \hat{T}_7(t) \\ \hat{T}_2(t) & \hat{T}_4(t) & \hat{T}_6(t) & \hat{T}_8(t) \end{bmatrix}^{\mathrm{T}} \begin{bmatrix} \cos\alpha_i(t) \\ \sin\alpha_i(t) \end{bmatrix}$, (33) and (34) are verified. ■

Theorems 4.2 and 4.3 provide the thrust force and the spin axis' tilt angle for each propeller so that the desired forces and moments are produced. However, since tilt-rotor quadcopters with H-configuration are underactuated, it is not always possible to find $T_i(\cdot)$, $i = 1, \ldots, 4$, and $\alpha_i(\cdot)$ that realize any arbitrary control input $u(\cdot)$. Indeed, (31) and (34) are solutions of least-squares optimization problems. This fact provides an additional challenge to the robustness of the proposed control law. Furthermore, imposing that $\alpha_1(t) = \alpha_2(t) = \alpha_3(t) = \alpha_4(t)$, $t \geq t_0$, further limits the propellers' ability to produce the desired forces and moments. For this reason, the propeller's thrust force $T_i^*(t)$, $t \geq t_0$, $i = 1, \ldots, 4$, given by (31) and the corresponding tilt-angle $\alpha_i(t)$ given by (32) produce forces and moments that approximate the desired control input better than the forces and moments produced by $T_i^*(t)$ and $\alpha_i(t)$ given by (34) and (35).

In the following section, we present robust MRAC laws for the virtual control input $w(\cdot)$ in (25).

V. ROBUST MODEL REFERENCE ADAPTIVE CONTROL

In this section, we consider feedback control laws for the virtual control input $w(\cdot)$ in the form

$$\gamma(q, \dot{q}, \hat{\Theta}) = -\Delta\Theta^{\mathrm{T}}\Phi(q, \dot{q}), \quad (q, \dot{q}, \hat{\Theta}) \in \mathcal{D} \times \mathbb{R}^6 \times \mathbb{R}^{39\times 6} \tag{36}$$

where $\Delta\Theta \triangleq \hat{\Theta} - \overline{\Theta}$ and $\overline{\Theta} \in \mathbb{R}^{39\times 6}$ denotes an estimate of Θ, that is, $\|\overline{\Theta} - \Theta\| \leq \varepsilon$ with $\varepsilon \geq 0$ arbitrarily small. The *adaptive gain matrix* $\hat{\Theta}(\cdot)$ is determined applying an MRAC framework so that the feedback-linearized trajectory tracking error dynamics (25) meets user-defined specifications.

The next theorem is the main original result of this section and provides an adaptive law for $\hat{\Theta}(\cdot)$ so that user-defined constraints on both the trajectory tracking error and the adaptive gains are verified, that is, $(e(t), \Delta\Theta(t)) \in \mathring{\mathcal{C}}$, $t \geq t_0$, where

$$\mathcal{C} \triangleq \left\{(e, \Delta\Theta) \in \mathbb{R}^{12} \times \mathbb{R}^{39\times 6} : h(e, \Delta\Theta) \geq 0\right\} \tag{37}$$

is bounded, connected, and denotes the *constraint set*

$$h(e, \Delta\Theta) \triangleq h_{\max} - \|M^{\frac{1}{2}}e\|^2 - \|\Delta\Theta\|^2_{\mathrm{F},\Gamma^{-1}}, \quad (e, \Delta\Theta) \in \mathbb{R}^{12} \times \mathbb{R}^{39\times 6} \tag{38}$$

$h_{\max} > 0$, $M^{\frac{1}{2}}$ denotes the square root of a symmetric and positive-definite solution $M \in \mathbb{R}^{12\times 12}$ of the Lyapunov inequality $A_{\mathrm{ref}}^{\mathrm{T}}M + MA_{\mathrm{ref}} \leq 0$, and $\Gamma \in \mathbb{R}^{39\times 39}$ is symmetric and positive-definite; note that $(0, 0) \in \mathring{\mathcal{C}}$. The constraint function (38) combines both the upper bound on the trajectory tracking error $e(\cdot)$ and the upper bound on the difference between the adaptive gain $\hat{\Theta}(\cdot)$ and the estimated gain $\overline{\Theta}$. Indeed, if $w(t) = \gamma(q(t), \dot{q}(t), \overline{\Theta})$, $t \geq t_0$, and the quadcopter dynamics were perfectly modeled, that is, $\overline{\Theta} = \Theta$ and $\xi(t) \equiv 0$, then the solution $e(\cdot)$ of (25) is such that $e(t) \to 0$ as $t \to \infty$. Therefore, the constraint set (37) allows us to bound both $\hat{\Theta}(\cdot)$ is some neighborhood of the estimated gain $\overline{\Theta}$ and $e(\cdot)$ in some neighborhood of the origin.

For the statement of the next theorem, define the barrier Lyapunov function candidate

$$V(e, \Delta\Theta) \triangleq \frac{e^{\mathrm{T}}Pe + \mathrm{tr}\left(\Delta\Theta^{\mathrm{T}}\Gamma^{-1}\Delta\Theta\right)}{h(e, \Delta\Theta)}, \quad (e, \Delta\Theta) \in \mathring{\mathcal{C}} \tag{39}$$

where $P \in \mathbb{R}^{12\times 12}$ denotes the symmetric, positive-definite solution of the algebraic Lyapunov equation

$$0 = A_{\mathrm{ref}}^{\mathrm{T}}P + PA_{\mathrm{ref}} + Q_1 \tag{40}$$

and $Q_1 \in \mathbb{R}^{12\times 12}$ is user-defined, symmetric, and positive-definite. Furthermore, let

$$\mathcal{S}_\Phi \triangleq \left\{(e, \Delta\Theta) \in \mathbb{R}^{12} \times \mathbb{R}^{39\times 6} : S_\Phi(e, \Delta\Theta) > 0\right\} \tag{41}$$

$$S_\Phi(e, \Delta\Theta) \triangleq -\alpha\|e\|^2 - \sigma\|e^{\mathrm{T}}PB\|^p\|\Delta\Theta\|^2_{\mathrm{F}} + 2\left(\varepsilon\|\Phi(q, \dot{q})\| + \xi_{\max}\right)\|\eta(e, \Delta\Theta)\| \tag{42}$$

where $p \in \mathbb{N}$, $\sigma > 0$, $\alpha \triangleq \lambda_{\min}(Q_1)$, $\xi_{\max} \geq 0$ is such that

$$\|\xi(t) + \left(\Theta - \overline{\Theta}\right)^{\mathrm{T}}\Phi(q(t), \dot{q}(t))\| \leq \xi_{\max}, \quad t \geq t_0 \tag{43}$$

and

$$\eta(e, \Delta\Theta) \triangleq e^{\mathrm{T}}\left[P + V(e, \Delta\Theta)M\right]B. \tag{44}$$

Finally, note that since both $q_{\mathrm{ref}}(t)$, $t \geq t_0$, and $\dot{q}_{\mathrm{ref}}(t)$ are bounded by assumption and $\mathcal{C}$ is compact, Both $q(\cdot)$ and $\dot{q}(\cdot)$ are bounded. Therefore, there exists a compact set $\mathcal{F} \subset \mathbb{R}^{39}$ such that $-\Phi(q(t), \dot{q}(t)) \in \mathcal{F}$ for all $t \geq t_0$, and, by the Weierstrass theorem [45, Th. 2.13],

$$\Phi^*(e, \Delta\Theta) \triangleq \mathrm{argmax}_{-\Phi\in\mathcal{F}} S_\Phi(e, \Delta\Theta), \quad (e, \Delta\Theta) \in \mathbb{R}^{12} \times \mathbb{R}^{39\times 6} \tag{45}$$

exists and is finite.

THEOREM 5.1 Consider the uncertain nonlinear dynamical system (25), the feedback control law (36), the constraint set (37), and the set $\mathcal{S}_\Phi$ given by (41). Let

$$\dot{\hat{\Theta}}^{\mathrm{T}}(t) = \Gamma\left[\Phi(q(t), \dot{q}(t))\eta(e(t), \Delta\Theta(t)) - \sigma\|e^{\mathrm{T}}(t)PB\|^p\Delta\Theta^{\mathrm{T}}(t)\right][1 + V(e(t), \Delta\Theta(t))]^{-1}$$
$$\hat{\Theta}(t_0) = \hat{\Theta}_0, \quad t \geq t_0 \tag{46}$$

where $P \in \mathbb{R}^{12\times 12}$ denotes the symmetric, positive-definite solution of (40), $V(\cdot, \cdot)$ is given by (39), and $\eta(\cdot, \cdot)$ is given by (44). If $w(t) = \gamma(q(t), \dot{q}(t), \hat{\Theta}(t))$, $t \geq t_0$, $(e(t_0), \Delta\Theta(t_0)) \in \mathring{\mathcal{C}}$, and $\mathcal{S}_{\Phi^*} \subset \mathring{\mathcal{C}}$, where $\Phi^*(\cdot, \cdot)$ is given by (45), then $(e(t), \Delta\Theta(t)) \in \mathring{\mathcal{C}}$, $t \geq t_0$.

PROOF The proof of this result follows by proceeding as in [46, The proof of Theorem 1] and is omitted for brevity. ■

The function $V(\cdot, \cdot)$ is a barrier Lyapunov function since it is positive-definite, decrescent along the trajectories of the dynamical system given by (25) and (46), and grows asymptotically, while approaching the boundary of the constraint set $\mathcal{C}$. These properties certify that the user-defined constraints are met along the trajectories of the closed-loop system.

The upper bound $\xi_{\max}$ in (43) can be determined as follows. The reference position $r^{\mathbb{I}}_{\mathrm{ref}}(t)$, $t \geq t_0$, is user-defined, and since $|\phi_{\mathrm{ref}}(t)|$, $|\theta_{\mathrm{ref}}(t)|$, $|\psi_{\mathrm{ref}}(t)| < 2\pi$, an upper bound on $\|q_{\mathrm{ref}}(t)\|$ can be readily computed. Furthermore, $\dot{r}^{\mathbb{I}}_{\mathrm{ref}}(t)$, $t \geq t_0$, $\dot{\theta}_{\mathrm{ref}}(t)$, $\dot{\psi}_{\mathrm{ref}}(t)$ are user-defined, and differentiating (12), we deduce that $|\dot{\phi}_{\mathrm{ref}}(t)| \leq |\frac{\mathrm{d}}{\mathrm{d}t}\frac{\tilde{v}_{\mathrm{tran},2}(t)}{\tilde{v}_{\mathrm{tran},3}(t)}|$. Now, $\tilde{v}_{\mathrm{tran},2}(t)$, $t \geq t_0$, and $\tilde{v}_{\mathrm{tran},3}(t)$ capture components of the thrust force in a reference frame obtained by rotating $\mathbb{J}(t)$ about $x(t)$ of an angle $\phi_{\mathrm{ref}}(t)$ and, since $\tilde{v}^2_{\mathrm{tran},3}(t) \geq \kappa^2$, an upper bound on

$$\left|\frac{\mathrm{d}}{\mathrm{d}t}\frac{\tilde{v}_{\mathrm{tran},2}(t)}{\tilde{v}_{\mathrm{tran},3}(t)}\right| = \left|\frac{\dot{\tilde{v}}_{\mathrm{tran},2}(t)\tilde{v}_{\mathrm{tran},3}(t) - \dot{\tilde{v}}_{\mathrm{tran},3}(t)\tilde{v}_{\mathrm{tran},2}(t)}{\tilde{v}^2_{\mathrm{tran},3}(t)}\right|$$

can be estimated from the design specifications of the propellers and their motors. Thus, an upper bound on $\|\dot{q}_{\mathrm{ref}}(t)\|$, $t \geq t_0$, can be computed. Next, it holds that $[q^{\mathrm{T}}(t), \dot{q}^{\mathrm{T}}(t)]^{\mathrm{T}} = e(t) + [q^{\mathrm{T}}_{\mathrm{ref}}(t), \dot{q}^{\mathrm{T}}_{\mathrm{ref}}(t)]^{\mathrm{T}}$, $t \geq t_0$, and it follows from (38) that $\|e(t)\| \leq \sqrt{h_{\max}}$. Hence, upper bounds on $\|q(t)\|$ and $\|\dot{q}(t)\|$ can be estimated. Similarly, upper bounds on $\|\ddot{q}(t)\|$, $t \geq t_0$ can be deduced from (25). Finally,

upper bounds on $\|\Delta f_{\text{dyn,tran}}(t,q,\dot{q})\|$, $(t,q,\dot{q}) \in [t_0,\infty) \times \mathcal{D} \times \mathbb{R}^n$, $\|\Delta f_{\text{dyn,rot}}(t,q,\dot{q})\|$, and $\|\Delta \mathcal{M}(t,q)\|$ are user-defined and capture the user's confidence to accurately model the system's dynamics by means of $\overline{f}_{\text{dyn,tran}}(t,q,\dot{q})$, $(t,q,\dot{q}) \in [t_0,\infty) \times \mathcal{D} \times \mathbb{R}^n$, $\overline{f}_{\text{dyn,rot}}(t,q,\dot{q})$, and $\overline{\mathcal{M}}(t,q)$, respectively. Thus, $\xi_{\max}$ can be computed by noting that $\|\xi(t)\| = \|\xi_{\text{dyn}}(t)\|$, $t \geq t_0$, and applying both the triangle inequality and the Cauchy–Schwarz inequality to the left-hand side of (43) and the right-hand-sides of (21), (22), and (26) with $u(\cdot)$ deduced from (14) and (16) and $v(t) = \beta(t, q(t), q_{\text{ref}}(t), \gamma(q(t), \dot{q}(t), \hat{\Theta}(t)))$.

A possible disturbance to the quadcopter's dynamics, which violates the assumptions underlying this article, involves adding or subtracting mass from the payload. This disturbance directly affects $\|\Delta \mathcal{M}(t,q)\|$, $(t,q,\dot{q}) \in [t_0,\infty) \times \mathcal{D} \times \mathbb{R}^6$, $\|\Delta f_{\text{dyn,tran}}(t,q,\dot{q})\|$, and $\|\Delta f_{\text{dyn,rot}}(t,q,\dot{q})\|$, and it can be accounted for by increasing $\xi_{\max}$. Errors in estimating the quadcopter's mass induce also systematic errors in the estimate of the quadcopter's inertia matrix $I(\cdot)$, namely $\overline{\overline{I}}$, and the position of its center of mass $r_C(\cdot)$, namely $\overline{\overline{r}}_C$. These parametric uncertainties are captured by $\overline{\overline{f}}_{\text{dyn,tran}}(q,\dot{q})$, $(q,\dot{q}) \in \mathcal{D} \times \mathbb{R}^6$, and $\overline{\overline{f}}_{\text{dyn,rot}}(q,\dot{q})$, and are compensated by the adaptive law (46). Similarly, the sloshing of fluids in the payload induces oscillatory variations in the overall system's inertia matrix and position of the center of mass. In this case, the average of these oscillatory disturbances provides a parametric uncertainty, which is compensated by the adaptive law (46), and the unsteady components of these disturbances can be accounted for by increasing $\xi_{\max}$.

The set $\mathcal{S}_{\Phi^*}$ captures the effect of uncertainties in the plant dynamics on the control law (36) and the adaptive law (46). The condition $\mathcal{S}_{\Phi^*} \subset \mathring{\mathcal{C}}$ can be enforced by minimizing the diameter of $\mathcal{S}_{\Phi^*}$, that is, choosing α and σ sufficiently large, and providing accurate estimates of Θ so that ε is small. The condition $\mathcal{S}_{\Phi^*} \subset \mathring{\mathcal{C}}$ can be also enforced by minimizing $\xi_{\max}$. The unknown function $\xi(\cdot)$ in (25) captures both unknown external disturbances and those terms in the system's dynamical model that are not well captured by the regressor vector $\Phi(\cdot,\cdot)$. Therefore, $\xi_{\max}$ can be minimized by carefully designing $\Phi(\cdot,\cdot)$; (19)–(24) provide a systematic approach, based on the analysis of the quadcopter's kinodynamic equations, to design the regressor vector. Alternative approaches to create accurate regressor vectors involve the use of neural networks [47]–[49].

If $\xi_{\max} = 0$, then Theorem 5.1 reduces to [46, Th. 1]; indeed, the results in [46] do not apply in the presence of unmatched uncertainties $\xi(\cdot)$. If $p = 1$, $\overline{\Theta} = 0$, and the constraints on both $e(\cdot)$ and $\Delta\Theta(\cdot)$ are neglected, that is, $h_{\max} \to \infty$, then Theorem 5.1 reduces to the *e*-modification of MRAC, which is stated in the following.

THEOREM 5.2 ([26]) Consider the uncertain nonlinear dynamical system (25) and the feedback control law (36). Let

$$\dot{\hat{\Theta}}^{\mathrm{T}}(t) = \Gamma \left(\Phi(q(t),\dot{q}(t))e^{\mathrm{T}}(t)PB - \sigma\|e^{\mathrm{T}}(t)PB\|\hat{\Theta}^{\mathrm{T}}(t)\right)$$
$$\hat{\Theta}(t_0) = \hat{\Theta}_0, \qquad t \geq t_0 \tag{47}$$

where $P \in \mathbb{R}^{12\times 12}$ denotes the symmetric, positive-definite solution of (40). If $w(t) = \gamma(q(t), \dot{q}(t), \hat{\Theta}(t))$, $t \geq t_0$, then the trajectory tracking error $e(\cdot)$ is uniformly ultimately bounded, and the adaptive gain matrix $\hat{\Theta}(\cdot)$ is uniformly bounded.

Theorem 5.2 presents a robust MRAC law that, in the presence of unmatched uncertainties, guarantees both uniform boundedness of $\hat{\Theta}(\cdot)$ and uniform ultimate boundedness of $e(\cdot)$, that is, boundedness of the trajectory tracking error after some finite-time transient, whose extent does not depend on the initial condition $t_0 \in [0,\infty)$. The bounds on $\|e(\cdot)\|$ and $\|\hat{\Theta}(\cdot)\|$, however, can only be estimated in a conservative manner and are functions of the upper bound $\xi_{\max}$ on the unmatched uncertainty. Since $\xi_{\max}$ can only be estimated, if the virtual control input $w(\cdot)$ in (25) is designed by applying Theorem 5.2, then user-defined bounds on both the trajectory tracking error and the adaptive gains can only be enforced by tuning Γ and σ iteratively. The advantage of applying Theorem 5.1 over Theorem 5.2 is that the user-defined constraints on both the trajectory tracking error $e(\cdot)$ and the adaptive gain matrix $\hat{\Theta}(\cdot)$ captured by (37) can be set explicitly and imposed *a priori* despite parametric, matched, and unmatched uncertainties in the trajectory tracking error dynamics.

VI. FLIGHT TESTS

In this section, we present the results of two flight tests and show the ability of the control strategy presented in Section IV and the robust MRAC laws presented in Section V to control both the position and the attitude of a tilt-rotor quadcopter. In particular, the first flight test involves the proposed adaptive law (46), and the second test involves the classical robust adaptive law (47). A video of the test involving the proposed adaptive law (46) is available at [11]. This video also shows that if the UAV's propellers are locked so that the aircraft becomes a classical quadcopter, then the mission is not accomplished.

A. Flight Test Setup

Both flight tests involve the same setup presented in this section. Specifically, the mass of the tilt-rotor quadcopter is 2.0 kg, and according to custom-made high-fidelity CAD model, its principal moments of inertia are $[0.0208, 0.0468, 0.0303]\,\text{kg}\cdot\text{m}^2$; the UAV is connected to a cart, whose mass is 6.2 kg and whose inertia matrix is unknown. The UAV's estimated moments of inertia serve also as estimates of the overall system's inertia matrix. The UAV's mission is to hover for $t \in [0,7]$ s, travel 2 m in the negative X-axis direction for $t \in [7,15]$ s, hover for $t \in [15,22]$s, travel 1 m in the positive X-axis direction for $t \in [22,26]$ s, hover for $t \in [26,30]$ s, and maintain a constant altitude of 1m and 0° pitch angle at all times.

As discussed in Section I, the UAV controllers' performances are challenged by the fact that a thin rope of unknown length, which is slack at $t = 0$ s, connects the aft edge of the tilt-rotor to a cart of unknown inertial properties.

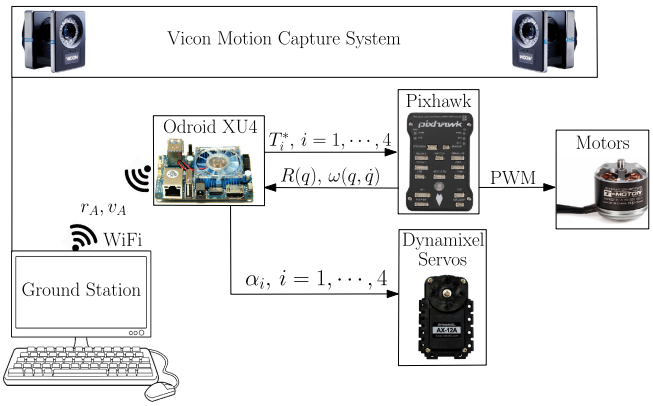

Fig. 3. Schematic representation of the flight test setup. A motion capture system is connected to a ground station computer, where the UAV's translational position and velocity are estimated. These data are transmitted to an ODroud XU4 single-board computer over WiFi. A Pixhawk autopilot, estimates the UAV's rotational position and velocity, which are communicated to the Odroid XU4 computer over a dedicated USB serial line. A numerical code programmed in C++ implements the control architecture outlined in Fig. 2 on the single-board computer.

Furthermore, numerical errors and communication delays further strain the aircraft's control algorithms.

In both flight tests, the gains of the proportional-derivative linear controller employed in (18) are

$$K_{\mathrm{P}} = \mathrm{diag}\left([4.0, 7.0, 5.5, 35, 20, 60]^{\mathrm{T}}\right)$$
$$K_{\mathrm{D}} = \mathrm{diag}\left([2.2, 2.0, 3.0, 9.0, 4.5, 10]^{\mathrm{T}}\right).$$

The user-defined constraints on the trajectory tracking error and the adaptive gains are captured by (37) with $h_{\max} = 185.50$ and $M = \mathbf{1}_{12}$. Furthermore, $p = 1$ in (46), and $\Gamma = 2 \cdot \mathbf{1}_{39}$, $Q_1 = \mathbf{1}_{12}$, and $\sigma = 10^{-5}$ in (40), (46), and (47). The goal of this article is to design an algorithm to control the position and attitude of a tilt-rotor quadcopter that is agnostic of its payload. In order to challenge the ability of the MRAC laws to impose user-defined bounds on the trajectory tracking error, the gain matrices K_{P} and K_{D} have been set *a priori*, according to our experience in autopilot design for conventional quadcopters, and have not been tuned. Since K_{P} and K_{D} characterize the baseline controller, tuning these gains implicitly provides the control system with information about the inertial properties of the platform, the cart, and the rope, which are unknown.

The architecture designed to execute the flight tests discussed in this section is schematically represented by Fig. 3 and is described in the following. A Vicon motion capture system is employed to deduce the UAV's position at 150 Hz with a precision of 10^{-3} m. This information is collected by a personal computer, which deduces the vehicle's velocity by applying Newton's first-order method. Successively, the aircraft's position and velocity are transmitted over WiFi signal to an ODroid XU4 single-board computer installed on the UAV. Merging data measured by an ST Micro L3GD20H gyroscope and an ST LSM303D accelerometer, the UAV's acceleration, angular position, and angular velocity are estimated by the PX4 flight software installed on a Pixhawk autopilot with accuracies of $\pm 0.05^\circ$, $\pm 3^\circ/\mathrm{s}$, and $\pm 7^\circ/\mathrm{s}^2$, respectively. The vehicle's angular position and velocity are then communicated to the single-board computer over a dedicated USB serial line. The single board computer acquires the UAV's translational position and velocity at approximately 200 Hz and the UAV's rotational position and velocity at approximately 400 Hz.

Data acquired by the UAV's single-board computer are employed to integrate either the proposed adaptive law (46) or the adaptive law (47) and compute both the feedback-linearizing control law (18) and the feedback control law (36); the sets of nonlinear differential equations (46) and (47) are integrated employing the Runge–Kutta method [50, Ch. 5]. Finally, the propellers' desired thrust force and the respective tilt angles are computed by applying either Theorem 4.2 or Theorem 4.3. All calculations are performed by a custom-made numerical code, which is programmed in C++ and executed at approximately 150 Hz by the ODroid XU4 computer.

The desired tilt angles $\alpha_i(\cdot)$, $i = 1, \ldots, 4$, are transmitted to Dynamixel AX-12 A servos over dedicated USB serial lines; these motors are characterized by an accuracy of 1° circa and provide position feedback as precise as 0.3°. It follows from (7) and (11) that the time derivative of the tilt angles is needed to deduce both the propellers' angular velocities and the time derivative of the moments of inertia. Thus, $\dot{\alpha}_i(\cdot)$, $i = 1, \ldots 4$, is computed by the ODroid computer by differentiating $\alpha_i(\cdot)$ numerically according to Newton's first-order method. The propellers' spin rates $\dot{\Omega}_i(\cdot)$, $i = 1, \ldots, 4$, are deduced from (27), where k is provided by the manufacturer, and $\Omega_i(\cdot)$, $i = 1, \ldots, 4$, which is needed to compute (7), is calculated by integrating $\dot{\Omega}_i(\cdot)$ employing Euler's first-order method and setting $\Omega_i(t_0) = 0$. To actuate the propellers, the desired thrust forces, $T_i^*(\cdot)$, $i = 1, \ldots, 4$, are sent via a USB serial line from the Odroid computer to the Pixhawk autopilot, which in turn sends pulsewidth modulation (PWM) signals to each motor.

It is worthwhile to note that the use of inexpensive sensors, the use of first-order forward differentiators to estimate the vehicle's translational velocity, the transmission of data over WiFi signal, and the lack of synchronization among the multiple measurements, sampling, differentiation, and integration algorithms involved in this architecture introduce several sources of errors that must be compensated by the adaptive laws employed to control the UAV [50, Ch. 3]. Furthermore, the PWM signal is a quadratic function of the thrust force [51], and as common practice in multirotor UAV applications, the Pixhawk autopilot assumes a linear relation deduced by considering the UAV's hover condition as the operative point. As shown in the following, the large weight of the cart requires the UAV motors to operate close to their saturation limits, which are far from the hover linearization point. This is an additional challenge to the robustness of the adaptive control laws employed in the proposed flight tests.

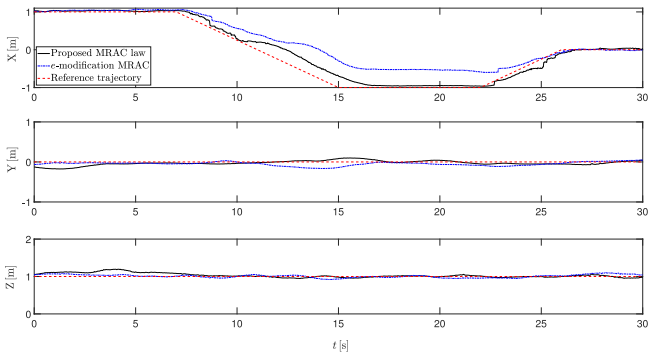

Fig. 4. Tilt-rotor quadcopter's actual and reference trajectories achieved by applying the adaptive laws (46) and (47).

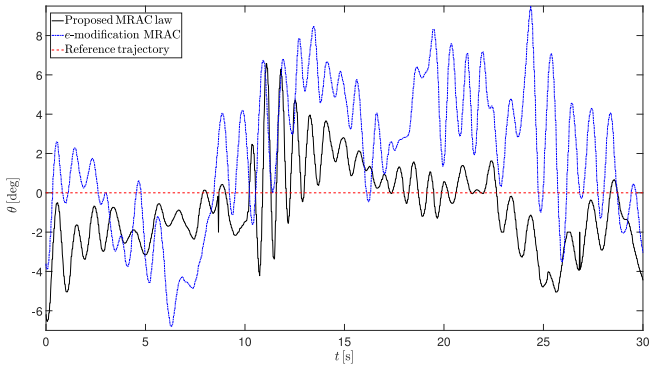

Fig. 5. Tilt-rotor quadcopter's pitch angle. Applying the *e*-modification of MRAC, the pitch angle deviates from the reference value of 0° more than applying the proposed constrained robust MRAC law.

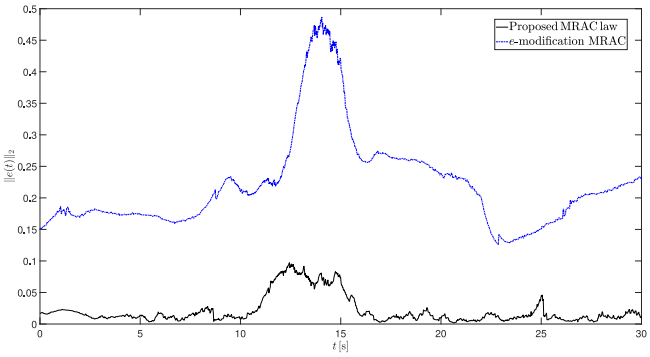

Fig. 6. Norms of the trajectory tracking errors obtained employing the proposed constrained, robust MRAC algorithm, and the *e*-modification of MRAC. Applying the *e*-modification of MRAC, the trajectory tracking error is larger than the error obtained applying the proposed MRAC law.

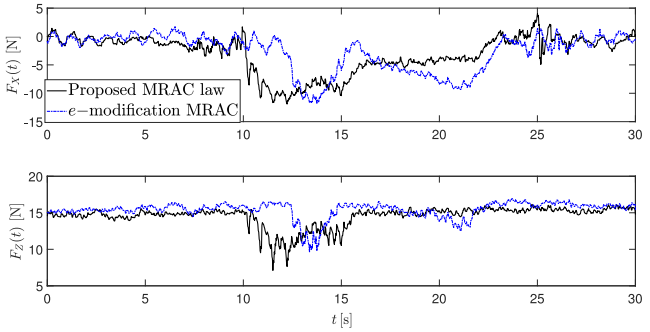

Fig. 7. Components of the thrust force produced by the quadcopter's propellers along the X and Z axes. In both flight tests, the propellers' spin axes are computed by applying Theorem 4.2.

B. Flight Tests Results

Fig. 4 shows the quadcopter's reference trajectory and the actual trajectories obtained applying (46) and (47). Applying the proposed adaptive law (46), the $\mathcal{L}_\infty$-norm of the position tracking error is 0.361 m, which is 54.30% smaller than the $\mathcal{L}_\infty$-norm of the position tracking error obtained applying the classical adaptive law (47). Moreover, applying the proposed adaptive law (46), the $\mathcal{L}_2$-norm of the position tracking error is 2.75 m, which is, 26.07% smaller than the $\mathcal{L}_2$-norm of the position tracking error obtained applying (47). Therefore, the proposed adaptive law (46) outperforms the classical adaptive law (47) by producing smaller position tracking error both pointwise and in average over the time.

Fig. 5 shows the pitch angle of the vehicle throughout the test. Applying both (46) and (47), the pitch angle tracking error experiences a sudden increase short after the rope is taut at 10.10 s. The $\mathcal{L}_\infty$- and $\mathcal{L}_2$-norms for the proposed law (46) are 6.58° and 15.89°, respectively. These values are 44.27% smaller and 82.73% smaller than the $\mathcal{L}_\infty$-norm and $\mathcal{L}_2$-norm of the pitch angle obtained applying (47), respectively.

Fig. 6 shows the normalized trajectory tracking error applying both (46) and (47). The $\mathcal{L}_\infty$- and the $\mathcal{L}_2$-norms of the trajectory tracking error $e(\cdot)$ obtained applying the proposed constrained adaptive law (46) are 299.18 and 59.67% smaller than the $\mathcal{L}_\infty$- and the $\mathcal{L}_2$-norms of the trajectory tracking error obtained applying the classical adaptive law (47), respectively. Interestingly, the trajectory tracking error induced by the proposed adaptive law (46) is characterized by a higher frequency content than the one induced by (47); this phenomenon may be due to having embedded a barrier Lyapunov function in the control algorithm.

Fig. 7 shows the components of the propellers' thrust force along the X and Z axes obtained by applying the adaptive laws (46) and (47). Applying (46), the $\mathcal{L}_\infty$- and $\mathcal{L}_2$-norms of the horizontal component of thrust force are 10.76 N and 55.30 N, respectively. These values are respectively 1.02 and 10.48% larger than the $\mathcal{L}_\infty$-norm and $\mathcal{L}_2$-norm of the horizontal component of thrust force obtained applying (47), respectively. Moreover, applying (46), the $\mathcal{L}_\infty$- and $\mathcal{L}_2$-norms of the vertical component of thrust force are 16.15 N and 168.00 N, which are respectively 4.90 and 5.93% smaller than the $\mathcal{L}_\infty$-norm and $\mathcal{L}_2$-norm of the vertical component of thrust force obtained applying (47), respectively. At $t = 10.10$ s, the rope connecting the quadcopter to the cart is taut and the thrust along the X axis must increase. Although both (47) and (46) are characterized by the same adaptive rates, the thrust force induced by (47) is delayed with respect to the reaction force induced by (46). As shown by Fig. 4, these different reaction times affect the position tracking error along the X axis.

Fig. 8 shows the percentage of the total available thrust required by both MRAC laws, that is, $\dfrac{\|T^*(t)\|}{T_{\max}}, t \geq 0$, where

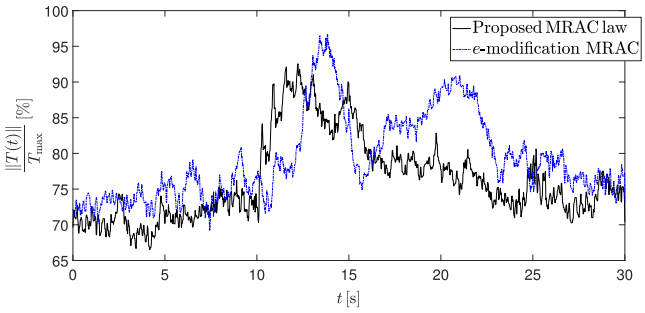

Fig. 8. Percentage of total available thrust used during both flight tests. The control algorithm based on the e-modification of MRAC generally uses more thrust throughout the mission than the control algorithm based on the proposed constrained, robust MRAC law.

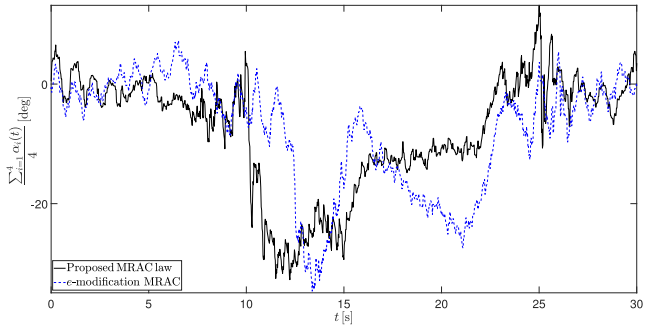

Fig. 9. Average tilt angles of the propellers's spin axes over the course of the flight tests. In both flight tests, the propellers' spin axes are computed by applying Theorem 4.2.

$T_{\max}$ denotes the maximum available thrust. Applying (46), the $\mathcal{L}_\infty$-norm of the thrust force is 92.56% and, applying (47), the $\mathcal{L}_\infty$-norm of the thrust force is 96.68%. These peaks occur at $t = 12.20$ s and $t = 13.85$ s, respectively. Furthermore, Fig. 8 shows how the proposed MRAC requires a stronger horizontal component of the thrust force than the e-modification of MRAC and hence, it better exploits the UAV's thrust vectoring capability. The Pixhawk autopilot employed for these flight experiments underlies a linear relation between PWM and thrust, which is deduced by assuming that the UAV requires 50% of the available thrust to perform its mission. However, both of the control laws require more than 90% of the available thrust, and hence, the realized thrust force may not match the desired thrust, and the robustness of the control laws is challenged.

Fig. 9 shows the average tilt angles of the propellers while implementing both the proposed adaptive law (46) and the robust MRAC law (47), allowing all propellers' spin axes to tilt independently. While the aircraft hovers and before the rope is taut, that is, for $t \in [0, 10.10]$ s, applying either adaptive law, the average tilt angle oscillates around 0° and, as shown by Fig. 5, the UAV's pitch angle is close to 0°. As soon as the rope is taut, the propellers' tilt angles experience a sudden decrease to exert some force along the negative X axis direction and, as shown by Fig. 9, applying the proposed adaptive law the tilt angles vary more rapidly

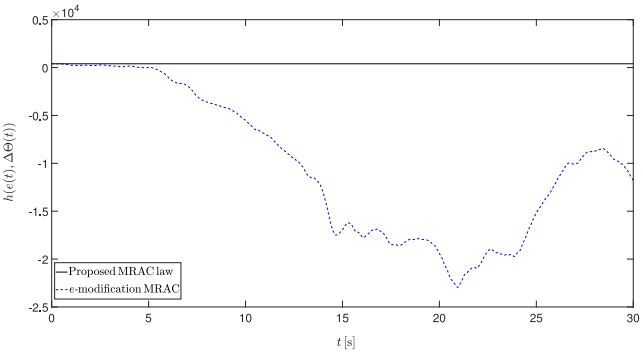

Fig. 10. Function characterizing the user-defined constraint on both the trajectory tracking error and the estimated adaptive gain's error. Applying the proposed robust MRAC law, $h(e(t), \Delta\Theta(t)) > 0$, $t \geq 0$ s, and hence, the user-defined constraints are never violated. Applying the e-modification of MRAC, $h(e(t), \Delta\Theta(t)) \leq 0$, $t \geq 4.6$ s, and hence, the user-defined constraints are violated.

TABLE I
Comparison of the Performances of the Proposed Adaptive law (46) and e-Modification of MRAC law (47)

	Eq. (46)	Eq. (47)	Difference
$\|r_A(t) - r_{\text{ref}}(t)\|_{\mathcal{L}_2}$	2.75m	3.46m	26.07%
$\|r_A(t) - r_{\text{ref}}(t)\|_{\mathcal{L}_\infty}$	0.36m	0.56m	54.30%
$\|\theta(t)\|_{\mathcal{L}_2}$	15.89°	28.48°	82.73%
$\|\theta(t)\|_{\mathcal{L}_\infty}$	6.58°	9.49°	44.27%
$\|e(t)\|_{\mathcal{L}_2}$	0.32	0.511	59.67%
$\|e(t)\|_{\mathcal{L}_\infty}$	0.12	0.49	299.18%
$\|F_X(t)\|_{\mathcal{L}_2}$	55.30N	49.50N	-10.48%
$\|F_X(t)\|_{\mathcal{L}_\infty}$	10.76N	10.65N	-1.02%
$\|F_Z(t)\|_{\mathcal{L}_2}$	168.00N	178.80N	5.93%
$\|F_Z(t)\|_{\mathcal{L}_\infty}$	16.15N	16.94N	4.90%
$\|T^*(t)\|_{\mathcal{L}_2}/\|T_{\max}\|_{\mathcal{L}_2}$	0.76	0.79	3.93%
$\|T^*(t)\|_{\mathcal{L}_\infty}/T_{\max}$	0.92	0.96	4.45%

than applying the e-modification of MRAC. During the second hover stage, that is, for $t \in [15, 22]$ s, applying the proposed adaptive law, the average tilt angle is smaller than applying the e-modification of MRAC. Indeed, as shown by Fig. 4, applying (46), the position tracking error is smaller than the position tracking error obtained applying (47). Furthermore, as shown by Fig. 7, in this stage the proposed adaptive law requires a smaller horizontal component of the thrust force than applying the e-modification of MRAC. For $t \geq 22$ s, that is, when the vehicle is no longer tasked with pulling the cart, the average tilt angle oscillates around 0°.

Lastly, Fig. 10 shows the constraint function $h(e(t), \Delta\Theta(t))$, $t \geq 0$ s. It is apparent that, applying the proposed robust MRAC law, $h(e(t), \Delta\Theta(t)) > 0$, $t \geq 0$ s, and hence, the given constraints are never violated. However, applying the e-modification of MRAC, $h(e(t), \Delta\Theta(t)) \leq 0$, $t \geq 4.6$ s, and hence, the user-defined constraints on the trajectory tracking error and estimated adaptive gain's error are violated.

Analyzing the results of these flight tests, we deduce that the proposed adaptive law (46) guarantees higher trajectory tracking performance than the adaptive law (47). Moreover, (46) induces a thrust force, whose maximum amplitude is

smaller than the one induced by (47), and whose average over time is similar to the one induced by (47). The performances of the two adaptive laws employed in these flight tests are summarized by Table I.

VII. CONCLUSION

This article presented a detailed analysis of the equations of motion of a tilt-rotor quadcopters with H-configuration, an innovative control architecture for these vehicles, and a novel robust MRAC law that allows us to enforce *a priori* user-defined constraints on both the trajectory tracking error and the adaptive gains. The effectiveness of the proposed results and their advantages over classical robust MRAC laws have been highlighted by flight tests. Future research directions involve the implementation of MRAC laws that constrain the control input directly, and not by bounding the adaptive gains. Additional future work directions involve outdoor flight tests, wherein the UAV pulls some cart on a rough terrain.

ACKNOWLEDGMENT

The authors would like to thank Mr. Harris L. Edge and Mr. James M. Dotterweich at the Vehicles Technology Directorate of ARL for their continuous collaboration.

REFERENCES

[1] D. K. D. Villa, A. S. B. ao, and M. Sarcinelli-Filho
A survey on load transportation using multirotor UAVs
J. Intell. Robot. Syst., vol. 80, pp. 267–296, 2020.

[2] D. R. McArthur, A. B. Chowdhury, and D. J. Cappelleri
Design of the interacting-boomcopter unmanned aerial vehicle for remote sensor mounting
J. Mech. Robot., vol. 10, no. 2, 2018, Art. no. 025001.

[3] W. Myeong and H. Myung
Development of a wall-climbing drone capable of vertical soft landing using a tilt-rotor mechanism
IEEE Access, vol. 7, pp. 4868–4879, 2019.

[4] C.-S. Yoo, B.-J. Park, A. Cho, and Y.-S. Kang
Simulation based on motion platform for tilt rotor UAV shipboard landing
In *Proc. Int. Conf. Control, Autom. Syst.*, 2015, pp. 1747–1750.

[5] F. Augugliaro *et al.*
The flight assembled architecture installation: Cooperative construction with flying machines
IEEE Control Syst. Mag., vol. 34, no. 4, pp. 46–64, Aug. 2014.

[6] H. Zhang, J. Zhang, G. Zong, W. Wang, and R. Liu
Sky cleaner 3: A real pneumatic climbing robot for glass-wall cleaning
IEEE Robot. Autom. Mag., vol. 13, no. 1, pp. 32–41, Mar. 2006.

[7] C. Papachristos, K. Alexis, and A. Tzes
Efficient force exertion for aerial robotic manipulation: Exploiting the thrust-vectoring authority of a tri-tiltrotor UAV
In *Proc. Int. Conf. Robot. Autom.*, 2014, pp. 4500–4505.

[8] A. Albers, S. Trautmann, T. Howard, T. A. Nguyen, M. Frietsch, and C. Sauter
Semi-autonomous flying robot for physical interaction with environment
In *Proc. IEEE Conf. Robot., Autom. Mechatronics*, 2010, pp. 441–446.

[9] Y. Long, L. Wang, and D. J. Cappelleri
Modeling and global trajectory tracking control for an overactuated MAV
Adv. Robot., vol. 28, no. 3, pp. 145–155, 2014.

[10] A. Nemati, R. Kumar, and M. Kumar
Stabilizing and control of tilting-rotor quadcopter in case of a propeller failure
In *Proc. Dyn. Syst. Control Conf*, 2016, Paper DSCC2016-9897.

[11] R. B. Anderson, J. A. Marshall, and A. L'Afflitto
Flight experiment of a tilt-rotor quadcopter pulling a poorly modeled cart
[Online]. Avaialble: https://youtu.be/RWD0ckn8iQM, 2019, Accessed: Apr. 17, 2020.

[12] C. Doniselli, M. Gobbi, and G. Mastinu
Measuring the inertia tensor of vehicles
Vehicle Syst. Dyn., vol. 37, no. sup. 1, pp. 301–313, 2002.

[13] A. L'Afflitto, R. B. Anderson, and K. Mohammadi
An introduction to nonlinear robust control for unmanned quadrotor aircraft: How to design control algorithms for quadrotors using sliding mode control and adaptive control techniques
IEEE Control Syst. Mag., vol. 38, no. 3, pp. 102–121, Jun. 2018.

[14] M. Ryll, H. H. Bülthoff, and P. R. Giordano
A novel overactuated quadrotor unmanned aerial vehicle: Modeling, control, and experimental validation
IEEE Trans. Control Syst. Technol., vol. 23, no. 2, pp. 540–556, Mar. 2015.

[15] A. T. Tran, N. Sakamoto, M. Sato, and K. Muraoka
Control augmentation system design for quad-tilt-wing unmanned aerial vehicle via robust output regulation method
IEEE Trans. Aerosp. Electron. Syst., vol. 53, no. 1, pp. 357–369, Feb. 2017.

[16] B. Yuksek, A. Vuruskan, U. Ozdemir, M. Yukselen, and G. Inalhan
Transition flight modeling of a fixed-wing VTOL UAV
J. Intell. Robot. Syst., vol. 84, no. 1–4, pp. 83–105, 2016.

[17] S. M. Nogar and C. M. Kroninger
Development of a hybrid micro air vehicle capable of controlled transition
IEEE Robot. Autom. Lett., vol. 3, no. 3, pp. 2269–2276, Jul. 2018.

[18] T. Wang, J. Wang, C. Wu, M. Zhao, and T. Ge
Disturbance-rejection control for the hover and transition modes of a negative-buoyancy quad tilt-rotor autonomous underwater vehicle
Appl. Sci., vol. 8, no. 12, 2018, Art. no. 2459.

[19] C. Yih
Flight control of a tilt-rotor quadcopter via sliding mode
In *Proc. Int. Autom. Control Conf.*, 2016, pp. 65–70.

[20] Y. Yildiz, M. Unel, and A. E. Demirel
Nonlinear hierarchical control of a quad tilt-wing UAV: An adaptive control approach
Int. J. Adapt. Control Signal Process., vol. 31, no. 9, pp. 1245–1264.

[21] E. D'Amato, G. D. Francesco, I. Notaro, G. Tartaglione, and M. Mattei
Nonlinear dynamic inversion and neural networks for a tilt trirotor UAV
In *Proc. IFAC Workshop Adv. Control Navig. Auton. Aerosp. Vehicles*, vol. 48, no. 9, 2015, pp. 162–167.

[22] D. Kastelan, M. Konz, and J. Rudolph
Fully actuated tricopter with pilot-supporting control
In *Proc. IFAC Workshop Adv. Control Navig. Autonom. Aerosp. Vehicles*, vol. 48, no. 9, 2015, pp. 79–84.

[23] S. Park, J. Bae, Y. Kim, and S. Kim
Fault tolerant flight control system for the tilt-rotor UAV
J. Franklin Inst., vol. 350, no. 9, pp. 2535–2559, 2013.

[24] C. Papachristos, K. Alexis, and A. Tzes
Dual–authority thrust–vectoring of a tri–tiltrotor employing model predictive control
J. Intell. Robot. Syst., vol. 81, nos. 3/4, pp. 471–504, 2016.

[25] R. Kumar, A. Nemati, M. Kumar, R. Sharma, K. Cohen, and F. Cazaurang
Tilting-rotor quadcopter for aggressive flight maneuvers using differential flatness based flight controller
In *Proc. ASME Dyn. Syst. Control Conf.*, vol. 3, 2006, pp. 1–7.

[26] K. Narendra and A. Annaswamy
A new adaptive law for robust adaptation without persistent excitation
IEEE Trans. Autom. Control, vol. 32, no. 2, pp. 134–145, Feb. 1987.

[27] Z. Liu, Y. He, L. Yang, and J. Han
Control techniques of tilt rotor unmanned aerial vehicle systems: A review
Chin. J. Aeronaut., vol. 30, no. 1, pp. 135–148, 2017.

[28] E. Lavretsky and K. Wise
Robust and Adaptive Control: With Aerospace Applications. London, U.K.: Springer, 2012.

[29] M. Ryll, H. Bülthoff, Heinrich, and P. R. Giordano
A novel overactuated quadrotor unmanned aerial vehicle: Modeling, control, and experimental validation
IEEE Trans. Control Syst. Technol., vol. 23, no. 2, pp. 540–556, Mar. 2015.

[30] C. Papachristos, K. Alexis, and A. Tzes
Design and experimental attitude control of an unmanned tilt-rotor aerial vehicle
In *Proc. Int. Conf. Adv. Robot.*, 2011, pp. 465–470.

[31] J. I. Giribet, R. S. Sanchez-Pena, and A. S. Ghersin
Analysis and design of a tilted rotor hexacopter for fault tolerance
IEEE Trans. Aerosp. Electron. Syst., vol. 52, no. 4, pp. 1555–1567, Aug. 2016.

[32] A. Oosedo, S. Abiko, S. Narasaki, A. Kuno, A. Konno, and M. Uchiyama
Flight control systems of a quad tilt rotor unmanned aerial vehicle for a large attitude change
In *Proc. IEEE Int. Conf. Robot. Autom.*, 2015, pp. 2326–2331.

[33] G. Kreisselmeier and K. Narendra
Stable model reference adaptive control in the presence of bounded disturbances
IEEE Trans. Autom. Control, vol. 27, no. 6, pp. 1169–1175, Dec. 1982.

[34] E. Arabi, B. C. Gruenwald, T. Yucelen, and N. T. Nguyen
A set-theoretic model reference adaptive control architecture for disturbance rejection and uncertainty suppression with strict performance guarantees
Int. J. Control, vol. 91, no. 5, pp. 1195–1208, 2018.

[35] T. Yucelen, G. D. L. Torre, and E. N. Johnson
Improving transient performance of adaptive control architectures using frequency-limited system error dynamics
Int. J. Control, vol. 87, no. 11, pp. 2383–2397, 2014.

[36] M. Sharifi, S. Behzadipour, and G. Vossoughi
Nonlinear model reference adaptive impedance control for human–robot interactions
Control Eng. Pract., vol. 32, pp. 9–27, 2014.

[37] R. B. Anderson, J. A. Marshall, J.-P. Burke, and A. L'Afflitto
Robust adaptive control of a tilt-rotor quadcopter with unknown inertial properties
In *Proc. Amer. Control Conf.*, 2019, pp. 2922–2927.

[38] H. K. Khalil
Nonlinear Systems, ser. Pearson Education. Princeton, NJ, USA: Prentice-Hall, 2002.

[39] D. S. Bernstein
Matrix Mathematics, 2nd ed. Princeton, NJ, USA: Princeton Univ. Press, 2009.

[40] A. L'Afflitto
A Mathematical Perspective on Flight Dynamics and Control. London, U.K.: Springer, 2017.

[41] A. L'Afflitto and K. Mohammadi
Equations of motion of rotary-wing UAS with time-varying inertial properties
AIAA J. Guid., Control, Dyn., vol. 41, no. 2, pp. 559–564, 2018.

[42] M. Hua, T. Hamel, P. Morin, and C. Samson
A control approach for thrust-propelled underactuated vehicles and its application to VTOL drones
IEEE Trans. Autom. Control, vol. 54, no. 8, pp. 1837–1853, Aug. 2009.

[43] R. Naldi, M. Furci, R. G. Sanfelice, and L. Marconi
Robust global trajectory tracking for underactuated VTOL aerial vehicles using inner-outer loop control paradigms
IEEE Trans. Autom. Control, vol. 62, no. 1, pp. 97–112, Jan. 2017.

[44] S. P. Boyd and L. Vandenberghe
Convex Optimization. Cambridge, U.K.: Cambridge Univ. Press, 2004.

[45] W. M. Haddad and V. Chellaboina
Nonlinear Dynamical Systems and Control: A Lyapunov-Based Approach. Princeton, NJ, USA: Princeton Univ. Press, 2008.

[46] A. L'Afflitto
Barrier Lyapunov functions and constrained model reference adaptive control
IEEE Control Syst. Lett., vol. 2, no. 3, pp. 441–446, Jul. 2018.

[47] N. Nguyen, K. Krishnakumar, and J. Boskovic
An Optimal Control Modification to Model-Reference Adaptive Control for Fast Adaptation, Honolulu, HI, USA, 2008.

[48] Z.-X. Yang, G.-S. Zhao, R.-J. Bao, H.-J. Rong, and L.-T. Gao
Robust kernel-based model reference adaptive control for unstable aircraft
Adv. Mech. Eng., vol. 8, no. 11, pp. 1–12, 2016.

[49] R. Prakash and R. Anita
Robust model reference adaptive intelligent control
Int. J. Control, Autom., Syst., vol. 10, pp. 396–406, 2012.

[50] W. Gautschi
Numerical Analysis. New York, NY, USA: Springer, 1997.

[51] A. Chovancová, T. Fico, L. Chovanec, and P. Hubinsk
Mathematical modelling and parameter identification of quadrotor (a survey)
Procedia Eng., vol. 96, no. 2014, pp. 172–181, 2014.

Robert B. Anderson received the B.S. degree in engineering physics and the M.S. degree in aerospace engineering from the University of Oklahoma, Norman, OK, USA, in 2017 and 2019, respectively. He is currently working toward the Ph.D. degree in industrial and systems engineering with Virginia Tech, Blacksburg, VA, USA.

Since 2016, he has been a part of the Advanced Control Systems Laboratory under Dr. L'Afflitto's advisement. His research interests include nonlinear robust control and integrated guidance and control systems with applications to autonomous robots and UAVs. He was recognized as one of the top 8 undergraduate student interns at the Army Research Laboratory in the summer of 2017.

Julius A. Marshall received the B.S. degree in aerospace engineering from the University of Oklahoma, Norman, OK, USA, in 2018. He is currently working toward the Ph.D. degree in industrial and systems engineering with Virginia Tech, Blacksburg, VA, USA.

Since 2018, he has been a part of the Advanced Control Systems Laboratory under Dr. L'Afflitto's advisement, where he is specializing in robotics. His current research interests include robust control, optimal control, guidance and navigation, and adaptive control for autonomous shipboard landing.

Mr. Marshall received the SMART Scholar Award in 2019.

Andrea L'Afflitto (Member, IEEE) received the B.S. degree in aerospace engineering and the M.S. degree in aerospace engineering and astronautics from the University of Napoli "Federico II," Naples, Italy, in 2004 and 2006, respectively, the M.S. degree in mathematics from Virginia Tech, Blacksburg, VA, USA, in 2010, and the Ph.D. degree in aerospace engineering from Georgia Tech, Atlanta, GA, USA, in 2015.

In 2019, he joined the Grado Department of Industrial and Systems Engineering, Virginia Tech, as an Assistant Professor, from 2015 to 2019, he was with the School of Aerospace and Mechanical Engineering, University of Oklahoma, as an Assistant Professor, and from 2008 to 2009 he was a System Engineer with the German Aerospace Agency, Cologne, Germany. His current research interests include nonlinear robust control, optimal control, and control of unmanned aerial systems.

Dr. L'Afflitto is a member of the IEEE Aerospace Controls Technical Committee. He received the DARPA Young Faculty Award in 2018.